# *Chapter 16*

# *Algorithms for the Navier-Stokes Equations - In 2-D Cartesian Coordinates*

## *16.1 Introduction*

This chapter presents and applies algorithms for solving the Navier-Stokes equations in two dimensional Cartesian coordinates. Before leaping into the complete Navier-Stokes equations it is wiser to build toward them by first solving subsets of these equations. In Chapter 5 the model parabolic equation, representing viscous diffusion, was solved. This equation is again used a building block for solving the N-S equations. Next the set of Thin Layer Navier-Stokes equations, which includes the main viscous terms for aerodynamic flow, is discussed and solved for Couette flow and then two dimensional flow past a flat plate. These basic computational building blocks are then assembled for solving the complete Navier-Stokes equations.

## *16.2 The Thin Layer Navier-Stokes Equations*

The Thin Layer Navier-Stokes (TLNS) equations, named by Baldwin and Lomax, represent an idealization of the full Navier-Stokes equations. This set retains the complete set of Euler terms and only the most significant viscous terms. In the hierarchy of governing equations it falls below Navier-Stokes, but above the boundary layer equations, because it includes all the terms of the Euler equations. A mesh for viscous flow past a flat plate is shown below, with the plate aligned with the *x* coordinate axis. The boundary layer along the plate for a high Reynolds number flow is very thin and requires a fine mesh in the direction normal to the wall for resolution. The mesh spacing in the stream direction is much coarser because of the slower change in the flow variables in this direction.

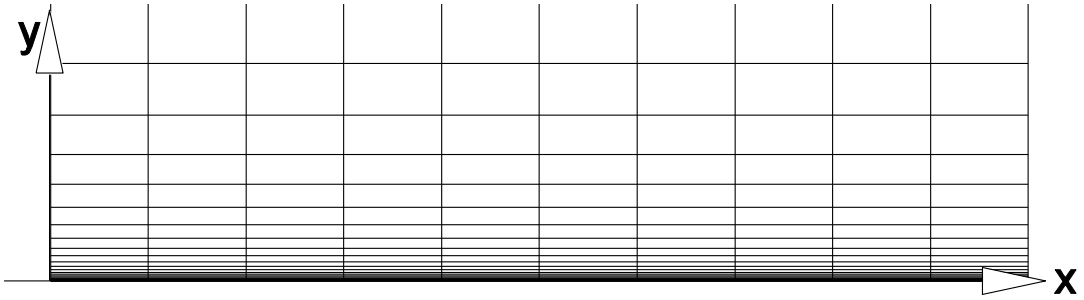


**Figure 16.1** Mesh for a viscous flow at high Reynolds number along a flat surface

For high Reynolds number flows, with body surfaces aligned with the $x$ axis, the $y$ derivative viscous terms are much more important than the $x$ derivative terms and are the only ones retained in the TLNS equations.

$$\left(\frac{\partial}{\partial y}\right)_{viscous} >> \left(\frac{\partial}{\partial x}\right)_{viscous}$$

Note that if the full set of Navier-Stokes equations were chosen for solution, only the pure *y* derivative viscous terms would receive proper support by the mesh shown in the above figure for a typical high Reynolds number aerodynamic flow. The choice is then to prune out the non-TLNS viscous terms from the Navier-Stokes equations or retain all the terms and let the mesh do the pruning instead. Nevertheless, we will use the TLNS equations as a start toward the solution of full Navier-Stokes equations. These equations are written in conservation law form as follows.

$$\frac{\partial U}{\partial t}+\frac{\partial F}{\partial x}+\frac{\partial G}{\partial y}=0$$

with $$U=\begin{bmatrix}\rho\\ \rho u\\ \rho v\\ e\end{bmatrix},\quad F=F_{Euler}=\begin{bmatrix}\rho u\\ \rho u^2+p\\ \rho vu\\ (e+p)u\end{bmatrix}$$

$$\text{and } G=G_{Euler}+G_{viscous}^{\text{tlns}}=\begin{bmatrix}\rho v\\ \rho uv\\ \rho v^2+p\\ (e+p)v\end{bmatrix}-\begin{bmatrix}0\\ \mu\dfrac{\partial u}{\partial y}\\ (\lambda+2\mu)\dfrac{\partial v}{\partial y}\\ u\mu\dfrac{\partial u}{\partial y}+v(\lambda+2\mu)\dfrac{\partial v}{\partial y}+k\dfrac{\partial T}{\partial y}\end{bmatrix}$$

The Thin Layer $G_{viscous}^{\text{tlns}}$ can be expressed as

$$G_{viscous}^{\text{tlns}}=-M_{yy}\frac{\partial V}{\partial y}=-\begin{bmatrix}0&0&0&0\\ 0&\mu&0&0\\ 0&0&\lambda+2\mu&0\\ 0&u\mu&v(\lambda+2\mu)&k\end{bmatrix}\frac{\partial}{\partial y}\begin{bmatrix}\rho\\ u\\ v\\ T\end{bmatrix}$$

## ***16.3 Implicit Algorithm for TLNS Equations***

An implicit algorithm for solving the TLNS equations, similar to that given earlier in Section 9.11, is give below. Note the matrix $N=\dfrac{\partial V}{\partial U}$ below used to convert $\delta V$ to $N\delta U$ .

$$\left\{ I + \alpha\Delta t \left( \frac{D_-\cdot}{\Delta x}\overline{A}^n_{+_{i+1/2,j}} + \frac{D_+\cdot}{\Delta x}\overline{A}^n_{-_{i-1/2,j}} + \frac{D_-\cdot}{\Delta y}\overline{B}^n_{+_{i,j+1/2}} + \frac{D_+\cdot}{\Delta y}\overline{B}^n_{-_{i,j-1/2}} \right) \right.$$
$$\left. -\Delta t \frac{D_-\cdot}{\Delta y} M_{yy_{i,j+1/2}} \frac{D_+\cdot}{\Delta y} N_{i,j} \right\} \delta U^{n+1}_{i,j} = \Delta U^n_{i,j}$$
$$= -\Delta t \left( \frac{F^n_{i+1/2,j} - F^n_{i-1/2,j}}{\Delta x} + \frac{G^n_{i,j+1/2} - G^n_{i,j-1/2}}{\Delta y} \right)_{Euler} \qquad (16.1)$$
$$+ \Delta t \frac{D_-\cdot}{\Delta y} M_{yy_{i,j+1/2}} \frac{D_+\cdot}{\Delta y} V_{i,j}$$

where again $\alpha = 1$ is used for first order flux approximations and $\alpha \geq \frac{3}{2}$ is recommended if higher order flux approximations are used on the right hand side of the equation. The Jacobian matrices $\overline{A}^n_+$, $\overline{A}^n_-$, $\overline{B}^n_+$ and $\overline{B}^n_-$ are defined as previously in Chapter 9 for the Euler equations and

$$N = \frac{\partial V}{\partial U} = \begin{bmatrix} 1 & 0 & 0 & 0 \\ -\frac{u}{\rho} & \frac{1}{\rho} & 0 & 0 \\ -\frac{v}{\rho} & 0 & \frac{1}{\rho} & 0 \\ \frac{u^2+v^2}{2c_v\rho} - \frac{T}{\rho} & -\frac{u}{c_v\rho} & -\frac{v}{c_v\rho} & \frac{1}{c_v\rho} \end{bmatrix}$$

Similarly, the block element matrices given Section 9.12.3 are now redefined as follows, where subscripts indicate locations as shown in Figure 16.2. See also Section 7.8 for discussion relating the mesh detail shown below for both finite difference and finite volume meshes and Section 11.4 for a discussion on the solution of two dimensional implicit matrix equations.

$$\overline{\mathrm{A}}_{i,j} = I + \frac{\Delta t}{\Delta x_i}\left( \alpha\overline{A}^n_{+_{i+1/2,j}} - \alpha\overline{A}^n_{-_{i-1/2,j}} \right)$$
$$+ \frac{\Delta t}{\Delta y_j}\left( \alpha\overline{B}^n_{+_{i,j+1/2}} - \alpha\overline{B}^n_{-_{i,j-1/2}} + \left( \frac{M_{yy_{i,j+1/2}}}{\Delta y_{j+1/2}} + \frac{M_{yy_{i,j-1/2}}}{\Delta y_{j-1/2}} \right) N_{i,j} \right),$$
$$\overline{\mathrm{B}}_{i,j} = \frac{\Delta t}{\Delta y_j}\left( +\alpha\overline{B}^n_{-_{i,j+1/2}} - \frac{1}{\Delta y_{j+1/2}} M_{yy_{i,j+1/2}} N_{i,j+1} \right), \qquad \overline{\mathrm{D}}_{i,j} = +\frac{\Delta t}{\Delta x_i}\alpha\overline{A}^n_{-_{i+1/2,j}}, \qquad (16.2)$$
$$\overline{\mathrm{C}}_{i,j} = \frac{\Delta t}{\Delta y_j}\left( -\alpha\overline{B}^n_{+_{i,j-1/2}} - \frac{1}{\Delta y_{j-1/2}} M_{yy_{i,j-1/2}} N_{i,j-1} \right) \text{ and } \overline{\mathrm{E}}_{i,j} = -\frac{\Delta t}{\Delta x_i}\alpha\overline{A}^n_{+_{i-1/2,j}}$$

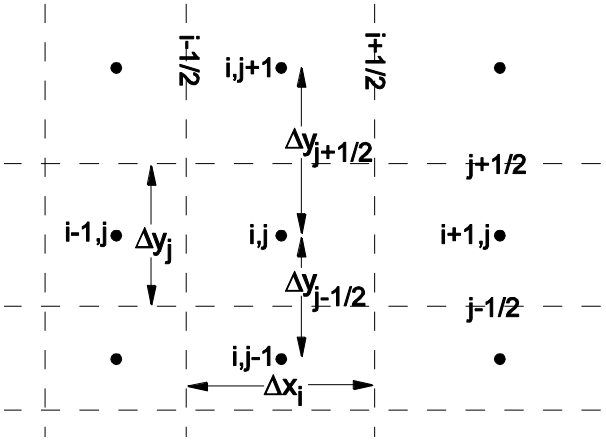


**Figure 16.2a** Mesh metric detail

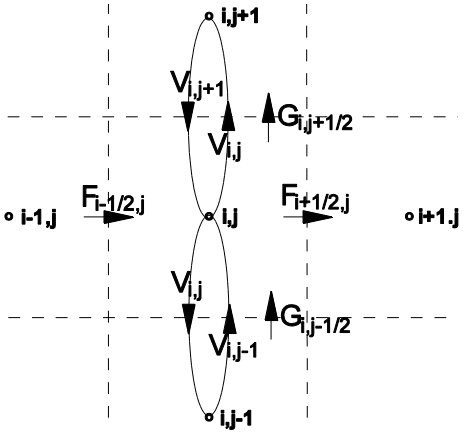


**b** Flux traffic pattern

The explicit flux is shown below, with the metric terms identified in Figure 16.2 a and the direction of the fluxes, both Euler and viscous, shown in Figure 16.2 b.

$$\Delta U_{i,j}^{n} = -\Delta t \left( \frac{F_{i+1/2,j}^{n} - F_{i-1/2,j}^{n}}{\Delta x_i} + \frac{G_{i,j+1/2}^{n} - G_{i,j-1/2}^{n}}{\Delta y_j} \right)_{Euler} + \frac{\Delta t}{\Delta y_j} \left( M_{yy_{i,j+1/2}} \frac{V_{i,j+1} - V_{i,j}}{\Delta y_{j+1/2}} - M_{yy_{i,j-1/2}} \frac{V_{i,j} - V_{i,j-1}}{\Delta y_{j-1/2}} \right)$$

## *16.4 Couette Flow*

Couette flow is the viscous flow between two infinite parallel flat plates a set distance apart, with one fixed and the other moving. This flow is shown in the figure below in the x-y plane.

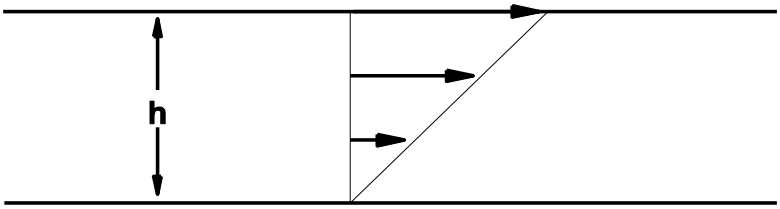


**Figure 16.3** Couette Flow

The top plate is moving with speed $u_{wall}$ and the plates are separated by distance $h$. All spatial derivatives in the governing Navier-Stokes equations vanish except those in the y direction. We may assume the flow to be incompressible for flow near Mach number zero. If we further assume that $\rho$ and coefficients $\mu$ and $k$ are constant and that the velocity in the $y$ direction $v = 0$, the equations reduce to just the following simplified $x$-momentum and energy equations

$$\frac{\partial u}{\partial t} = \frac{\mu}{\rho} \frac{\partial^2 u}{\partial y^2}$$

$$c_v \frac{\partial T}{\partial t} = \frac{\mu}{\rho} \left( \frac{\partial u}{\partial y} \right)^2 + \frac{k}{\rho} \frac{\partial^2 T}{\partial y^2}$$

If we assume that the flow goes to a steady state, $\frac{\partial^2 u}{\partial y^2} = 0 \Rightarrow u = ay + b$, where $a$ and $b$ are constants to be determined by the boundary conditions, $u = 0$ at $y = 0$ and $u = u_{wall}$ at $y = h$. Therefore, $u = \frac{u_{wall}}{h} y$ and $\frac{\partial u}{\partial y} = \frac{u_{wall}}{h}$. The equation for temperature will have a steady state if $-k\frac{\partial^2 T}{\partial y^2} = \mu\left(\frac{\partial u}{\partial y}\right)^2 = \mu\left(\frac{u_{wall}}{h}\right)^2$, which implies that the heat created by the term $\mu\left(\frac{\partial u}{\partial y}\right)^2$ must be carried away by conduction. By integration $T = -\frac{\mu}{2k}\left(\frac{u_{wall}}{h}\right)^2 y^2 + dy + e$, where $d$ and $e$ are constants to be determined by the boundary conditions.

***For isothermal wall boundary conditions,*** $T = T_{wall,0}$ at $y = 0$ and $T = T_{wall,h}$ at $y = h$, which yields $T = -\frac{\mu}{2k}\left(\frac{u_{wall}}{h}\right)^2 y^2 + \left(\frac{T_{wall,h} - T_{wall,0}}{h} + \frac{\mu h}{2k}\left(\frac{u_{wall}}{h}\right)^2\right) y + T_{wall,0}$

***For adiabatic wall boundary conditions,*** $\frac{\partial T}{\partial y} = 0$ at both $y = 0$ and $y = h$. But, $\frac{\partial T}{\partial y} = -\frac{\mu}{k}\left(\frac{u_{wall}}{h}\right)^2 y + d$, which implies $d = 0$ and $d = \frac{\mu}{k}\left(\frac{u_{wall}}{h}\right)^2 h$, an impossibility for Couette flow. Therefore *no steady state solution exists for the adiabatic wall case*. If we assume that $\frac{\partial T}{\partial t}$ is constant, then $\frac{\partial^2 T}{\partial y^2} = \frac{\rho c_v}{k}\frac{\partial T}{\partial t} - \frac{\mu}{k}\left(\frac{\partial u}{\partial y}\right)^2 = f$ and $\frac{\partial T}{\partial y} = fy + g$, where $f$ and $g$ are constants. When determined by the boundary conditions they become $f = g = 0$, which implies that the rate of growth of temperature is given by $\frac{\partial T}{\partial t} = \frac{\mu}{\rho c_v}\left(\frac{\partial u}{\partial y}\right)^2$ and $\frac{\partial T}{\partial y} = 0$ across the channel.

## ***16.4.1 Exercise: The Dimensional Diffusion Equation***

Solve the model parabolic equation in the form of the Couette flow $x$-momentum equation shown above. (Note: the diffusion equation shown below is essentially the same as the model parabolic equation discussed in Section 5.5.) Assume uniform flow between the plates at $t = t_0$, $u(y, t_0) = 1$ for $0 < y < h = 1$. At the boundaries $u(0, t) = 0$ and $u(h, t) = 1$ for all $t$. Span the space between the plates with $\Delta y = h/10$ and assume the kinematic viscosity $\nu = \mu/\rho = 0.05$.

$$\frac{\partial u}{\partial t} = \nu \frac{\partial^2 u}{\partial y^2}$$

***Numerical Method***

$$\left\{1-\alpha\nu\Delta t\frac{D_+}{\Delta y}\frac{D_-}{\Delta y}\cdot\right\}\delta u_j^{n+1}=\nu\Delta t\frac{D_+}{\Delta y}\frac{D_-}{\Delta y}\cdot u_j^n$$

where

$$\alpha=\begin{Bmatrix}0, & fully\ explicit, & stable\ if\quad \Delta t\le\Delta y^2/(2\nu)\\ 1/2, & Crank-Nicolson & \\ 1, & fully\ implicit & stable\ for\ all\quad \alpha\ge 1/2\end{Bmatrix},\quad O((1/2-\alpha)\Delta t,\Delta t^2,\Delta y^2)$$

***Cases***

(1) Set the time step for the fully explicit method to the maximum allowed for 100 time steps. (2) For the implicit method with $\alpha=1/2$, use $\Delta t=40$ for 10 time steps and (3) for $\alpha=1$ use $\Delta t=10^9$ for 1 time step.

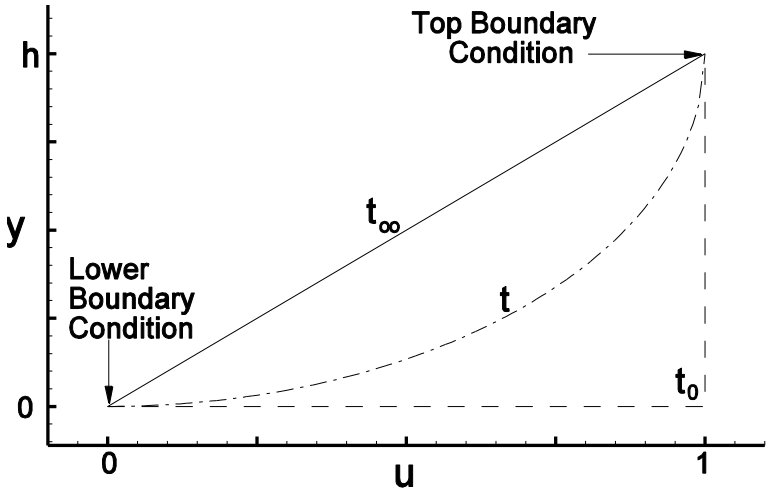


**Figure 16.4** Initial value problem for the Couette x-momentum equation

***Matrix Equation to be Solved***

The matrix equations to be solved and the grid point locations are shown below for both finite difference and finite volume approaches. Note that one more grid point is used in the finite volume approach to represent the two finite volumes outside the flow volume. These finite volumes are often called "ghost cells". Also note that the finite difference approach places grid points on the plate surfaces and the finite volume approach places volume cell boundaries along plate surfaces. This causes the difference in the implementation of the no slip boundary conditions within the matrix equations for the two approaches.

*Finite Difference Approach:*

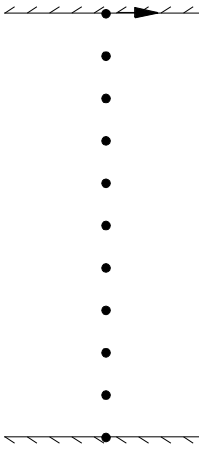

**Figure 16.5**
Finite difference grid

The matrix equation to be solved, including boundary conditions is, with $J = 11$,

$$\begin{bmatrix} 1 & 0 & 0 & 0 & 0 & 0 & 0 \\ b_{J-1} & a_{J-1} & c_{J-1} & 0 & 0 & 0 & 0 \\ 0 & \ddots & \ddots & \ddots & 0 & 0 & 0 \\ 0 & 0 & b_j & a_j & c_j & 0 & 0 \\ 0 & 0 & 0 & \ddots & \ddots & \ddots & 0 \\ 0 & 0 & 0 & 0 & b_2 & a_2 & c_2 \\ 0 & 0 & 0 & 0 & 0 & 0 & 1 \end{bmatrix} \begin{bmatrix} \delta u_J^{n+1} \\ \delta u_{J-1}^{n+1} \\ \vdots \\ \delta u_j^{n+1} \\ \vdots \\ \delta u_2^{n+1} \\ \delta u_1^{n+1} \end{bmatrix} = \begin{bmatrix} 0 \\ \Delta u_{J-1}^n \\ \vdots \\ \Delta u_j^n \\ \vdots \\ \Delta u_2^n \\ 0 \end{bmatrix}$$

with boundary conditions $u_1^n = 0$, $u_J^n = 1$ and $\delta u_1^n = \delta u_J^n = 0$.

*Finite Volume Approach:*

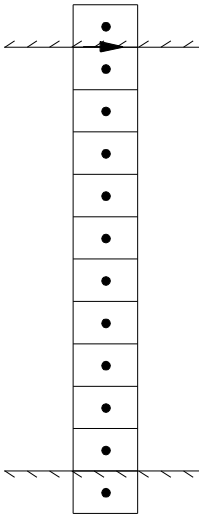

**Figure 16.6**
Finite volume grid

The matrix equation to be solved, including boundary conditions is, with $J = 12$,

$$\begin{bmatrix} 1 & 1 & 0 & 0 & 0 & 0 & 0 \\ b_{J-1} & a_{J-1} & c_{J-1} & 0 & 0 & 0 & 0 \\ 0 & \ddots & \ddots & \ddots & 0 & 0 & 0 \\ 0 & 0 & b_j & a_j & c_j & 0 & 0 \\ 0 & 0 & 0 & \ddots & \ddots & \ddots & 0 \\ 0 & 0 & 0 & 0 & b_2 & a_2 & c_2 \\ 0 & 0 & 0 & 0 & 0 & 1 & 1 \end{bmatrix} \begin{bmatrix} \delta u_J^{n+1} \\ \delta u_{J-1}^{n+1} \\ \vdots \\ \delta u_j^{n+1} \\ \vdots \\ \delta u_2^{n+1} \\ \delta u_1^{n+1} \end{bmatrix} = \begin{bmatrix} 0 \\ \Delta u_{J-1}^n \\ \vdots \\ \Delta u_j^n \\ \vdots \\ \Delta u_2^n \\ 0 \end{bmatrix}$$

with boundary conditions $u_1^n = -u_2^n$, $u_J^n = 2 - u_J^n$, $\delta u_1^n = -\delta u_2^n$ and $\delta u_J^n = -\delta u_{J-1}^n$.

For both approaches $a_j = 1 + 2\alpha \dfrac{\Delta t \nu}{\Delta y^2}$, $b_j = c_j = -\alpha \dfrac{\Delta t \nu}{\Delta y^2}$ and $\Delta u_j^n = \nu \Delta t \dfrac{D_+}{\Delta y} \cdot \dfrac{D_-}{\Delta y} \cdot u_j^n$

***Exercise Results***

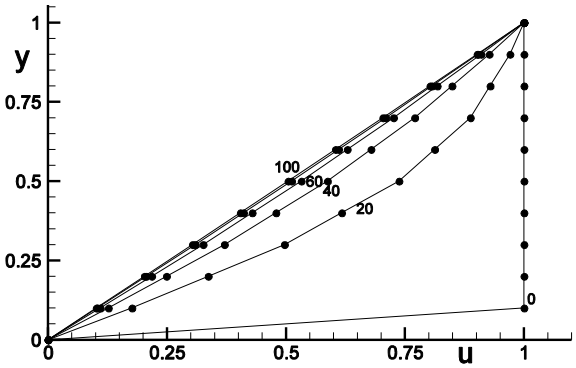


**Figure 16.7 (a)** Explicit, 100 steps, $\Delta t = \dfrac{\Delta x^2}{2\nu}$

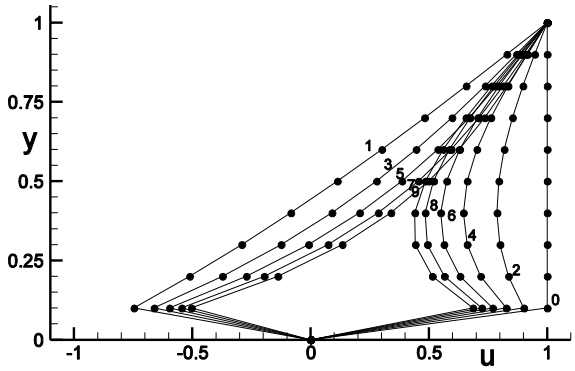


**(b)** Crank-Nicolson, 10 steps, $\Delta t = 40$

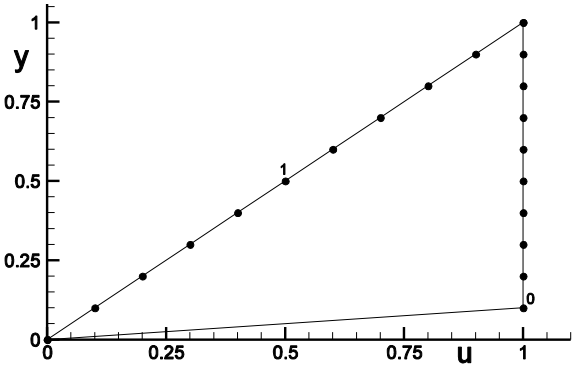


**Figure 16.7 (c)** Fully Implicit, 1 step, $\Delta t = 10^9$

## *16.4.2 Exercise : The Couette Flow Problem*

Solve the Thin Layer Navier-Stokes equations, shown below, for Couette flow.

$$\frac{\partial U}{\partial t} = -\frac{\partial F_e}{\partial x} - \frac{\partial G_e}{\partial y} + \frac{\partial M_{yy}\dfrac{\partial V}{\partial y}}{\partial y}$$

***Numerical Method:***

Treat only the viscous terms implicitly. Treat the Euler terms with either the Modified Steger Warming or Roe methods. Use Sutherland's law to compute the viscous coefficients (Section 15.2). Embed the viscous wall boundary conditions within the matrix equation to be solved. Use periodic boundary conditions in the stream-wise direction over length $L = 10m$. The distance between the parallel plates is $h = 10^{-10} m.$

*Note:* The distance $h$ was chosen small enough to provide a meaningful exercise in which the viscous terms dominant the Euler terms under standard aerodynamic conditions. However, this distance $h$ is so small that not even a hydrogen atom can pass freely between the plates, thus demonstrating that numerical simulation is less limited than experimental simulation.

***Initial Conditions:***

at $t = t_0$, $u(y,t_0) = 10m/s$, $p(y,t_0) = 10^5 N/m^2$ *and* $T(y,t_0) = 300^o K$, *for* $0 < y < h$

***Plate Boundary Conditions:***

The bottom plate is stationary at a temperature of $300^o K$. The top plate is moving with speed $10m/s$ and has temperature $310^o K$

***Cases:***

Calculate each case, (1) an isothermal wall case and (2) an adiabatic wall case, for 10 time steps, with $\Delta x = \frac{L}{2}$ and $\Delta y = \frac{h}{10}$, using the maximum time step allowed.

## *Solution Approach*

***The Mesh:***

The 4x12 finite volume mesh or the 4x11 finite difference mesh shown below uses the first and last columns for entrance and exit boundary conditions. The top and bottom rows, $j = 1$ and $j = J$, are boundary points for the wall boundaries. The flow values at the two interior mesh point columns should remain equal during the calculation and serve as an error check. The mesh points are located at the volume centers for the finite volume mesh and at the grid line intersections for the finite difference mesh. Note that the finite difference grid lines are also finite volumes mesh lines. The latter mesh is an extension of the former to provide "ghost cell" volumes.

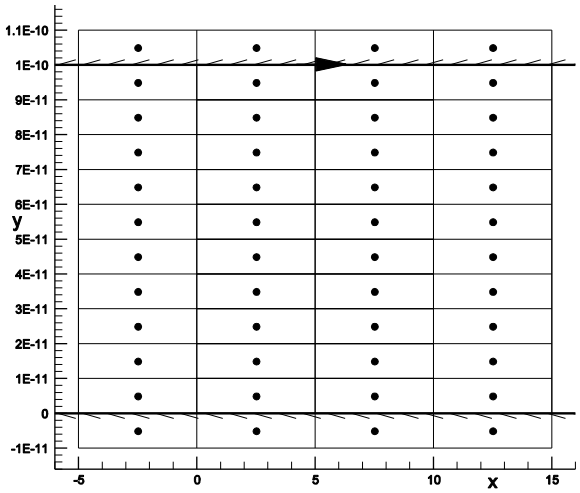


**Figure 16.8a** Finite volume mesh

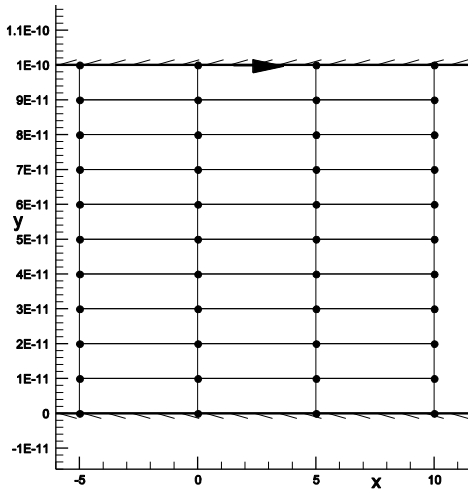


**Figure 16.8b** Finite difference mesh

***Time Step Size:***

The time step size for an explicit method solving the Navier-Stokes equations is found by searching for the minimum value for $\Delta t$ by the equation below over all interior mesh points $i, j$.

$$\Delta t \le \min_{i,j}\left\{\frac{1}{\frac{|u_{i,j}|}{\Delta x}+\frac{|v_{i,j}|}{\Delta y}+c_{i,j}\sqrt{\frac{1}{\Delta x^2}+\frac{1}{\Delta y^2}}+2\nu_{i,j}\left(\frac{1}{\Delta x^2}+\frac{2}{\Delta x\Delta y}+\frac{1}{\Delta y^2}\right)}\right\}, \qquad (16.3)$$

$$\text{where } \nu = \max\left\{\frac{\mu}{\rho}, \frac{k}{\rho c_v}\right\}$$

But, for laminar flow of air $\frac{k}{\rho c_v} = \frac{\gamma\mu}{\Pr_l \rho} \approx \frac{1.4\mu}{0.7\rho} = 2\frac{\mu}{\rho}$. Thus $\nu \approx \frac{2\mu}{\rho}$. Also, because only the pure $y$ derivative viscous terms are retained in the Thin Layer Navier-Stokes equations, and even those are to be treated implicitly, the time step size criterion becomes

$$\Delta t \le \min_{i,j}\left\{\frac{1}{\frac{|u_{i,j}|}{\Delta x}+\frac{|v_{i,j}|}{\Delta y}+c_{i,j}\sqrt{\frac{1}{\Delta x^2}+\frac{1}{\Delta y^2}}+\frac{4\mu_{i,j}}{\rho_{i,j}}\left(\cancel{\frac{1}{\Delta x^2}}+\cancel{\frac{2}{\Delta x\Delta y}}+\cancel{\frac{1}{\Delta y^2}}\right)}\right\}$$

$$\text{or} \quad \Delta t \le \min_{i,j}\left\{\frac{1}{\frac{|u_{i,j}|}{\Delta x}+\frac{|v_{i,j}|}{\Delta y}+c_{i,j}\sqrt{\frac{1}{\Delta x^2}+\frac{1}{\Delta y^2}}}\right\}$$

***Implicit Algorithm:***

The algorithm treating only the viscous term implicitly is, for each index $2 \le i \le I-1$ and $2 \le j \le J-1$,

$$U_{i,j}^{n+1} - U_{i,j}^{n} = -\Delta t\left(\frac{F_{e,\,i+1/2,j}^{\;n} - F_{e,i-1/2,j}^{n}}{\Delta x} + \frac{G_{e,i,j+1/2}^{n} - G_{e,i,j-1/2}^{n}}{\Delta y}\right) + \Delta t \frac{D_{-}\cdot}{\Delta y} M_{yy_{i,j+1/2}} \frac{D_{+}\cdot}{\Delta y} V_{i,j}^{n+1}$$

In delta law form, using $\delta U_{i,j}^{n+1} = U_{i,j}^{n+1} - U_{i,j}^{n}$ and $\delta V_{i,j}^{n+1} = V_{i,j}^{n+1} - V_{i,j}^{n}$, we obtain

$$\delta U_{i,j}^{n+1} - \Delta t \frac{D_{-}\cdot}{\Delta y} M_{yy_{i,j+1/2}} \frac{D_{+}\cdot}{\Delta y} \delta V_{i,j}^{n+1} = \left\{I - \Delta t \frac{D_{-}\cdot}{\Delta y} M_{yy_{i,j+1/2}} \frac{D_{+}\cdot}{\Delta y} N_{i,j}\right\} \delta U_{i,j}^{n+1} = \Delta U_{i,j}^{n+1}$$

$$= -\Delta t\left(\frac{F_{e,\,i+1/2,j}^{\;n} - F_{e,i-1/2,j}^{n}}{\Delta x} + \frac{G_{e,i,j+1/2}^{n} - G_{e,i,j-1/2}^{n}}{\Delta y}\right) + \Delta t \frac{D_{-}\cdot}{\Delta y} M_{yy_{i,j+1/2}} \frac{D_{+}\cdot}{\Delta y} V_{i,j}^{n}$$

The resulting matrix equation to be solved for each index $i$ becomes

$$\begin{bmatrix} \ddots & \ddots & \ddots & & \\ & B_{i,j} & A_{i,j} & C_{i,j} & \\ & & \ddots & \ddots & \ddots \end{bmatrix} \begin{bmatrix} \delta U_{i,j+1}^{n+1} \\ \delta U_{i,j}^{n+1} \\ \delta U_{i,j-1}^{n+1} \end{bmatrix} = \begin{bmatrix} \\ \Delta U_{i,j}^{n} \\ \\ \end{bmatrix}$$

where $B_{i,j} = -\frac{\Delta t}{\Delta y^2} M_{yy_{i,j+1/2}} N_{i,j+1}$, $C_{i,j} = -\frac{\Delta t}{\Delta y^2} M_{yy_{i,j-1/2}} N_{i,j-1}$ and

$$A_{i,j} = I + \frac{\Delta t}{\Delta y^2}(M_{yy_{i,j+1/2}} + M_{yy_{i,j-1/2}}) N_{i,j}$$

***Boundary Conditions for the Viscous Terms:***

***At the lower wall -*** the no slip condition implies that the fluid velocity is zero. The boundary conditions for both the finite difference and finite volume approaches are given below (see Section 12.6.3).

*Finite Difference Approach*

$$V_{i,1} = \begin{bmatrix} \rho \\ u \\ v \\ T \end{bmatrix}_{i,1} = \begin{bmatrix} \rho_{i,2} \\ 0 \\ 0 \\ tT_{i,2} + (1-t)T_{wall_1} \end{bmatrix} \text{ and } \delta V_{i,1} = \frac{\partial V_{i,1}}{\partial V_{i,2}} \delta V_{i,2} = E_1^{fd} \delta V_{i,2}, \text{ with } E_1^{fd} = \begin{bmatrix} 1 & 0 & 0 & 0 \\ 0 & 0 & 0 & 0 \\ 0 & 0 & 0 & 0 \\ 0 & 0 & 0 & t \end{bmatrix}$$

$$\text{where } t = \begin{cases} 1, & adaibatic\ \ wall \\ 0, & isothermal\ \ wall \end{cases}$$

Note: The boundary condition for the continuity equation above, $\rho_{i,1} = \rho_{i,2}$, is chosen for convenience, but is unnecessary because the matrix $M_{yy}$ has only zeros in the first column. A boundary condition of $\rho_{i,1} = 10^9 \rho_{i,2}$ would serve as well.

*Finite Volume Approach*

$$V_{i,1} = \begin{bmatrix} \rho \\ u \\ v \\ T \end{bmatrix}_{i,1} = \begin{bmatrix} \rho_{i,2} \\ -u_{i,2} \\ -v_{i,2} \\ tT_{i,2} + (1-t)T_{wall_1} \end{bmatrix} \text{ and } \delta V_{i,1} = \frac{\partial V_{i,1}}{\partial V_{i,2}} \delta V_{i,2} = E_1^{fv} \delta V_{i,2}, \text{ with } E_1^{fv} = \begin{bmatrix} 1 & 0 & 0 & 0 \\ 0 & -1 & 0 & 0 \\ 0 & 0 & -1 & 0 \\ 0 & 0 & 0 & t \end{bmatrix}$$

$$\text{where } t = \begin{cases} 1, & adaibatic\ \ wall \\ -1, & isothermal\ \ wall \end{cases}$$

We can combine the two approaches by defining $E_1 = \begin{bmatrix} 1 & 0 & 0 & 0 \\ 0 & e & 0 & 0 \\ 0 & 0 & e & 0 \\ 0 & 0 & 0 & t \end{bmatrix}$, where $t$ is defined as above for either the finite difference or finite volume approaches, whichever is appropriate, and

$$e = \begin{cases} 0, \ finite \ \ difference \\ -1, \ \ finite \ \ volume \end{cases}$$

*Embedding the lower boundary condition within the matrix equation*

The bottom two lines of the matrix equation are, where we make use of the relation $\delta V_{i,j}^{n+1} = N_{i,j} \delta U_{i,j}^{n+1}$,

$$\left.\begin{aligned} B_{i,2}\delta U_{i,3}^{n+1} + A_{i,2}\delta U_{i,2}^{n+1} - \frac{\Delta t}{\Delta y^2} M_{yy_{i,2-1/2}} \delta V_{i,1}^{n+1} = \Delta U_{i,2}^{n} \\ -E_1 \delta V_{i,2}^{n+1} + \delta V_{i,1}^{n+1} = 0 \end{aligned}\right\} \Rightarrow B_{i,2}\delta U_{i,3}^{n+1} + A'_{i,2}\,\delta U_{i,2}^{n+1} = \Delta U_{i,2}^{n}$$

$$\text{where } A'_{i,2} = I + \frac{\Delta t}{\Delta y^2}(M_{yy_{i,2+1/2}} + M_{yy_{i,2-1/2}}(I - E_1))N_{i,2}$$

***At the upper wall -*** the no slip condition implies that the fluid velocity is the same as that of the moving plate. The boundary conditions for both the finite difference and finite volume approaches are given below.

*Finite Difference Approach*

$$V_{i,J} = \begin{bmatrix} \rho \\ u \\ v \\ T \end{bmatrix}_{i,J} = \begin{bmatrix} \rho_{i,J-1} \\ u_{wall_J} \\ 0 \\ tT_{i,J-1} + (1-t)T_{wall_J} \end{bmatrix} \text{ and } \delta V_{i,J} = \frac{\partial V_{i,J}}{\partial V_{i,J-1}} \delta V_{i,J-1} = E_J^{fd} \delta V_{i,J-1}, \text{ with } E_J^{fd} = \begin{bmatrix} 1 & 0 & 0 & 0 \\ 0 & 0 & 0 & 0 \\ 0 & 0 & 0 & 0 \\ 0 & 0 & 0 & t \end{bmatrix}$$

$$\text{where } t = \begin{cases} 1, \ adaibatic \ \ wall \\ 0, \ isothermal \ \ wall \end{cases}$$

*Finite Volume Approach*

$$V_{i,J} = \begin{bmatrix} \rho \\ u \\ v \\ T \end{bmatrix}_{i,J} = \begin{bmatrix} \rho_{i,J-1} \\ -u_{i,J-1} + 2u_{wall_J} \\ -v_{i,J-1} \\ tT_{i,J-1} + (1-t)T_{wall_J} \end{bmatrix} \text{ and } \delta V_{i,1} = \frac{\partial V_{i,1}}{\partial V_{i,2}} \delta V_{i,2} = E_1^{fv} \delta V_{i,2}, \text{ with } E_J^{fv} = \begin{bmatrix} 1 & 0 & 0 & 0 \\ 0 & -1 & 0 & 0 \\ 0 & 0 & -1 & 0 \\ 0 & 0 & 0 & t \end{bmatrix}$$

$$\text{where } t = \begin{cases} 1, \ adaibatic \ \ wall \\ -1, \ isothermal \ \ wall \end{cases}$$

Again, we can combine the two approaches by defining $E_J = \begin{bmatrix} 1 & 0 & 0 & 0 \\ 0 & e & 0 & 0 \\ 0 & 0 & e & 0 \\ 0 & 0 & 0 & t \end{bmatrix}$, where $t$ is defined as above for either the finite difference or finite volume approaches, whichever is appropriate, and

$$e = \begin{cases} 0, \ finite \ \ difference \\ -1, \ \ finite \ \ volume \end{cases}$$

*Embedding the upper boundary condition within the matrix equation*

The top two lines of the matrix equation are, where we make use of the relation $\delta V_{i,j}^{n+1} = N_{i,j} \delta U_{i,j}^{n+1}$,

$$\left.\begin{aligned} \delta V_{i,J}^{n+1} - E_1 \delta V_{i,J-1}^{n+1} &= 0 \\ -\frac{\Delta t}{\Delta y^2} M_{yy_{i,J-1/2}} \delta V_{i,J}^{n+1} + A_{i,J-1} \delta U_{i,J-1}^{n+1} + C_{i,J-1} \delta U_{i,J-2}^{n+1} &= \Delta U_{i,J-1}^{n} \end{aligned}\right\} \Rightarrow A'_{i,J-1} \delta U_{i,J-1}^{n+1} + C_{i,2} \delta U_{i,J-2}^{n+1} = \Delta U_{i,J-1}^{n}$$

$$\text{where } A'_{i,J-1} = I + \frac{\Delta t}{\Delta y^2} (M_{yy_{i,J-1/2}} (I - E_J) + M_{yy_{i,J-3/2}}) N_{i,J-1}$$

The full tridiagonal matrix equation, to be solved for each interior mesh point column $i$, becomes

$$\begin{bmatrix} A'_{i,J-1} & C_{i,J-1} & & & & & & \\ B_{i,J-2} & A_{i,J-2} & C_{i,J-2} & & & & & \\ & \ddots & \ddots & \ddots & & & & \\ & & B_{i,j} & A_{i,j} & C_{i,j} & & & \\ & & & \ddots & \ddots & \ddots & & \\ & & & & B_{i,3} & A_{i,3} & C_{i,3} & \\ & & & & & B_{i,2} & A'_{i,2} \end{bmatrix} \begin{bmatrix} \delta U_{i,J-1}^{n+1} \\ \vdots \\ \delta U_{i,j+1}^{n+1} \\ \delta U_{i,j}^{n+1} \\ \delta U_{i,j-1}^{n+1} \\ \vdots \\ \delta U_{i,2}^{n+1} \end{bmatrix} = \begin{bmatrix} \Delta U_{i,J-1}^{n} \\ \vdots \\ \\ \Delta U_{i,j}^{n} \\ \\ \vdots \\ \Delta U_{i,2}^{n} \end{bmatrix}$$

***Boundary Conditions for the Euler Terms:***

***At solid walls*** - The velocity component normal to the wall vanishes, which implies "all you need is $p$" if the equations are written in conservation form. For the present problem of Couette flow the walls have no curvature and the boundary condition becomes simply $\frac{\partial p}{\partial y} = 0$. There is no real need to use the Modified Steger-Warming or Roe algorithm to evaluate the Euler flux at the walls. Therefore, we simply use

***At the lower wall*** - $p_{i,1} = p_{i,2}$ and $G_{e_{i,lower\ wall}} = \begin{bmatrix} 0 \\ 0 \\ p_{i,2} \\ 0 \end{bmatrix}$

***At the upper wall*** - $p_{i,J} = p_{i,J-1}$ and $G_{e_{i,upper\ wall}} = \begin{bmatrix} 0 \\ 0 \\ p_{i,J-1} \\ 0 \end{bmatrix}$

***At the entrance and exit boundaries***- The flow is assumed to be periodic over length $L$. The boundary conditions are therefore

$$U_{1,j} = U_{I-1,j} \text{ and } U_{I,j} = U_{2,j} \text{ , for all } 2 \le j \le J-1$$

The flow leaving across the surface at $x = L$ also enters across the surface at $x = 0$.

***Solutions:***

The time step size was calculated to be $\Delta t \approx 2.89 \times 10^{-14}$ and the initial Mach number was $M = \frac{u_{wall}}{c} \approx 0.029$. For *the adiabatic wall case* $\frac{\partial T}{\partial t} = \frac{\mu}{\rho c_v}\left(\frac{\partial u}{\partial y}\right)^2 \approx 2.2152 \times 10^{14}$, which implies an increase in temperature of $\Delta t \frac{\partial T}{\partial t} \approx 6.4^o K$ per time step. The results from the finite volume approach are shown below.

(1) Isothermal Wall Case, finite volume approach

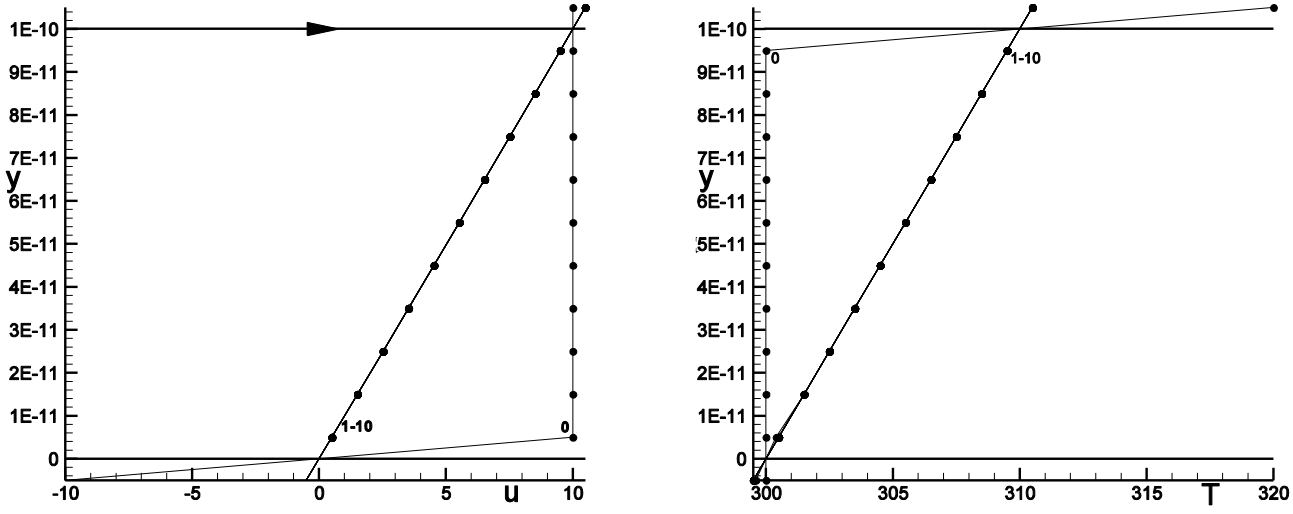


**Figure 16.9(a)** Velocity profiles **(b)** Temperature profiles

(2) Adiabatic Wall Case, finite volume approach

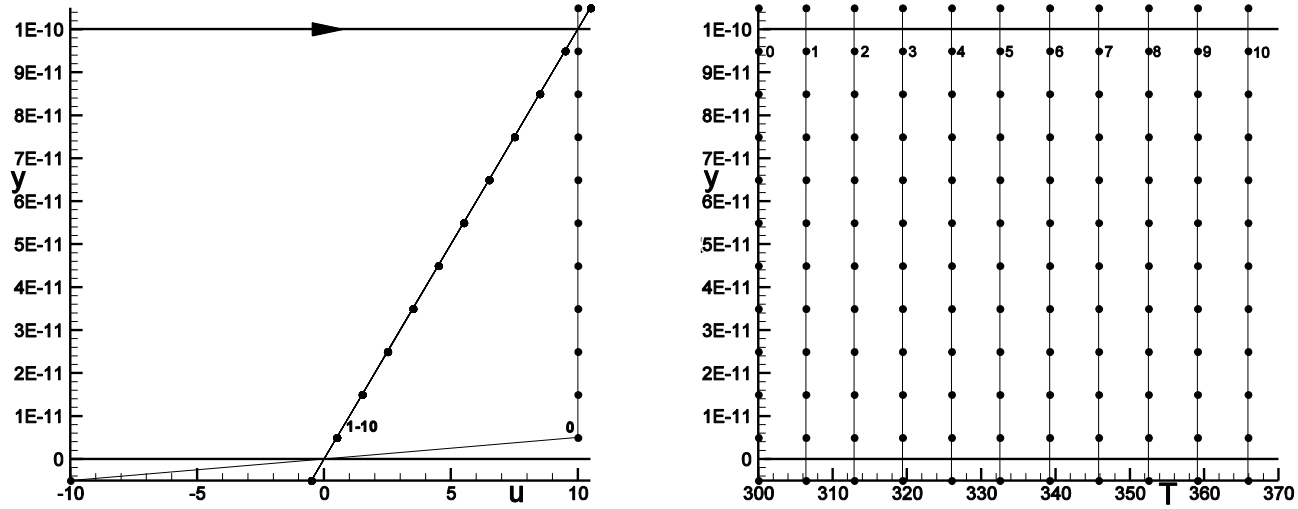


**Figure 16.10(a)** Velocity profiles **(b)** Temperature profile

## *16.5 The Blasius Boundary Layer*

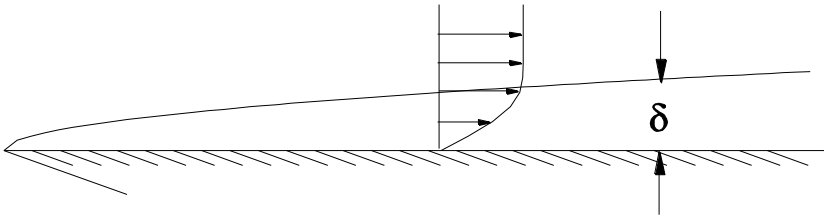


**Figure 16.11** Boundary layer on a flat plate

The velocity distribution within an incompressible laminar boundary layer along a flat plate was studied by Blasius in 1908. A similarity solution to the boundary layer equations was found using a cleaver coordinate transformation (see White, F.M., *Viscous Fluid Flow*, 3rd. Ed., McGraw-Hill). The incompressible boundary layer equations for continuity and x-momentum are

$$\frac{\partial u}{\partial x}+\frac{\partial v}{\partial y}=0$$

$$u\frac{\partial u}{\partial x}+v\frac{\partial u}{\partial y}=\nu\frac{\partial^2 u}{\partial y^2}$$

The kinematic viscosity $\nu$ is constant. The origin of the $x$ and $y$ coordinate system is located at the leading edge of the float plate. The boundary conditions are $u=v=0$ at $y=0$ along the plate surface and $u=u_\infty$, the free stream velocity, as $y\to\infty$. A stream function $\psi$ is introduced, such that $\frac{\partial\psi}{\partial x}=-v$ and $\frac{\partial\psi}{\partial y}=u$, to reduce the above equations to a single equation in a single unknown.

$$\frac{\partial \psi}{\partial y}\frac{\partial^2 \psi}{\partial x \partial y} - \frac{\partial \psi}{\partial x}\frac{\partial^2 \psi}{\partial y^2} = \nu \frac{\partial^3 \psi}{\partial y^3}$$

The boundary layer thickness $\delta$ is observed to grow with $\sqrt{x}$. Blasius scaled the y-coordinate by $\sqrt{x}$, to yield a dimensionless coordinate $\eta = y\sqrt{\frac{u_\infty}{\nu x}}$ and reduce the number of independent variables to one. The partial derivatives of $\eta$ are

$$\frac{\partial \eta}{\partial x} = -\frac{1}{2}\frac{y}{x}\sqrt{\frac{u_\infty}{\nu x}} = -\frac{1}{2}\frac{\eta}{x} \quad \text{and} \quad \frac{\partial n}{\partial y} = \sqrt{\frac{u_\infty}{\nu x}} = \frac{n}{y}$$

The similarity solution sought by Blasius was such that the velocity profile across the boundary layer could be expressed, for all $x$ locations downstream of the plate leading edge, by a single function of $\eta$, $u(x,y) = u_\infty u'(\eta)$. The stream function $\psi$ is defined by

$$\psi(x,y) = \int_0^y u(x,y')dy'\Big|_x = \int_0^\eta u_\infty u'(\eta')\sqrt{\frac{\nu x}{u_\infty}}d\eta'\Big|_x = \sqrt{u_\infty \nu x}\underbrace{\int_0^\eta u'(\eta')d\eta'}_{f(\eta)} = \sqrt{u_\infty \nu x}\, f(\eta)$$

Then, where the primes shown below designate differentiation with respect to $\eta$,

$$\frac{\partial \psi}{\partial x} = \frac{1}{2}\sqrt{\frac{u_\infty \nu}{x}}(f - \eta f'), \qquad \frac{\partial \psi}{\partial y} = u_\infty f',$$

$$\frac{\partial^2 \psi}{\partial x \partial y} = -\frac{1}{2}u_\infty \frac{\eta}{x} f'', \quad \frac{\partial^2 \psi}{\partial^2 y} = u_\infty \sqrt{\frac{u_\infty}{\nu x}} f'' \quad \text{and} \quad \frac{\partial^3 \psi}{\partial y^3} = \frac{u_\infty^2}{\nu x} f'''$$

Upon substitution of these derivatives of $\psi$ into the x-momentum equation, the following ordinary differential equation is obtained for $f(\eta)$.

$$f f'' + 2f''' = 0$$

with boundary conditions $f = f' = 0$ at $\eta = 0$ and $f' = 1$ as $\eta \to \infty$

Blasius presented a power series to approximate the solution to the above problem. But we can use the finite difference approach taken in these notes to approximate the solution as follows. We first reformulate the Blasius equation by letting $\phi = f'$. Then

$$f\frac{\partial \phi}{\partial \eta} + 2\frac{\partial^2 \phi}{\partial \eta^2} = 0 \text{ and } f(\eta) = \int_0^\eta \phi d\eta' = \int_0^\eta u'(\eta')d\eta'$$

which we approximate on an equi-spaced mesh $\eta_j = (j-1)\Delta\eta,\ j = 1,2,3\cdots,J$, by

$$f_j^n \frac{\phi_{j+1}^{n+1} - \phi_{j-1}^{n+1}}{2\Delta\eta} + 2\frac{\phi_{j+1}^{n+1} - 2\phi_j^{n+1} + \phi_{j-1}^{n+1}}{\Delta\eta^2} = 0,$$

$$\text{where } f_1^n = 0 \text{ and } f_j^n = f_{j-1}^n + \frac{1}{2}(\phi_j^n + \phi_{j-1}^n)\Delta\eta, \quad j = 2,\cdots,J,$$

with boundary conditions $\phi_1^n = 0$ at $\eta = 0$ and $\phi_J^n = 1$ at $\eta_J = (J-1)\Delta\eta$ for sufficiently large $\eta_J$.

## *16.5.1 Exercise: Solve The Blasius Equation*

We solve this non-linear equation by iteration on the index $n$. Choose $\Delta\eta = 0.1$ and $J = 90$

***Initial Condition:*** $\phi_j^0 = \min\{1,(j-1)\Delta\eta\}$, for $j = 1,\cdots,J$

***Matrix Equation:***

Solve the following tri-diagonal matrix equation for $n = 1,2,3\cdots,N = 5\,steps$ until convergence.

$$\begin{bmatrix} 1 & 0 & 0 & 0 & 0 & 0 & 0 \\ b_{J-1} & a_{J-1} & c_{J-1} & 0 & 0 & 0 & 0 \\ 0 & \ddots & \ddots & \ddots & 0 & 0 & 0 \\ 0 & 0 & b_j & a_j & c_j & 0 & 0 \\ 0 & 0 & 0 & \ddots & \ddots & \ddots & 0 \\ 0 & 0 & 0 & 0 & b_2 & a_2 & c_2 \\ 0 & 0 & 0 & 0 & 0 & 0 & 1 \end{bmatrix} \begin{bmatrix} \phi_J^{n+1} \\ \phi_{J-1}^{n+1} \\ \vdots \\ \phi_j^{n+1} \\ \vdots \\ \phi_2^{n+1} \\ \phi_1^{n+1} \end{bmatrix} = \begin{bmatrix} 1 \\ 0 \\ \vdots \\ 0 \\ \vdots \\ 0 \\ 0 \end{bmatrix},$$

$$\text{where } b_j = f_j^n + \frac{4}{\Delta\eta},\ a_j = \frac{-8}{\Delta\eta} \text{ and } c_j = -f_j^n + \frac{4}{\Delta\eta}, \text{ for } j = 2,\cdots,J-1$$

The solution is therefore $u_j = u_\infty \phi_j$ at $\eta_j = (j-1)\Delta\eta,\ j = 1,2,3\cdots,J$

***Results:***

The convergence of the solution to steady state is shown in the figure below. As seen, the results converge quickly to a steady velocity profile. We will use in the next section the converged Blasius velocity profile for comparison with the computed results for laminar flow past a flat plate at low Mach number described by the TLNS equations. A tabular representation of the velocity profile data is given in the table below.

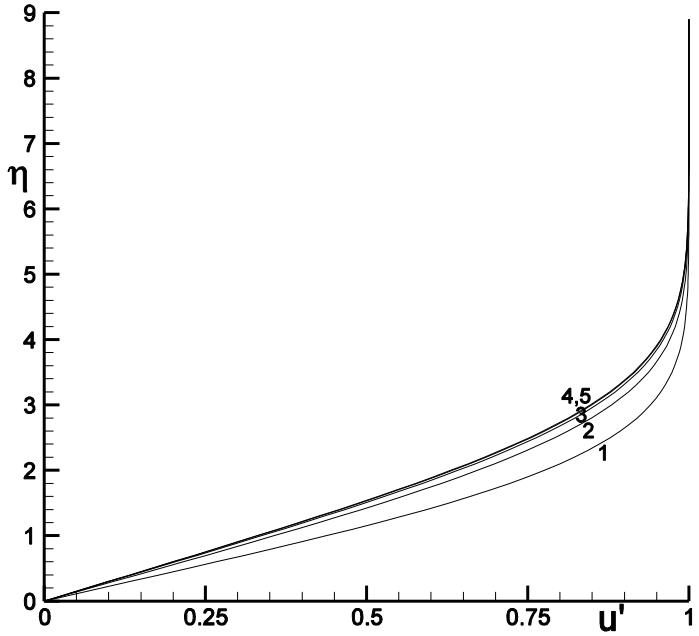


**Figure 16.12** Convergence of Blasius velocity profiles, for $n = 1, 2, 3, 4, 5$, $u' = u / u_\infty = \phi$

Table: Blasius Velocity Profile Data

| $\eta$ | $u'$ | $\eta$ | $u'$ | $\eta$ | $u'$ | $\eta$ | $u'$ | $\eta$ | $u'$ |
|---|---|---|---|---|---|---|---|---|---|
| 0.0 | 0.0000 | 1.5 | 0.4878 | 3.0 | 0.8471 | 4.5 | 0.9799 | 6.0 | 0.9990 |
| 0.1 | 0.0333 | 1.6 | 0.5178 | 3.1 | 0.8626 | 4.6 | 0.9830 | 6.1 | 0.9992 |
| 0.2 | 0.0665 | 1.7 | 0.5472 | 3.2 | 0.8771 | 4.7 | 0.9857 | 6.2 | 0.9994 |
| 0.3 | 0.0998 | 1.8 | 0.5759 | 3.3 | 0.8904 | 4.8 | 0.9880 | 6.3 | 0.9995 |
| 0.4 | 0.1330 | 1.9 | 0.6038 | 3.4 | 0.9026 | 4.9 | 0.9900 | 6.4 | 0.9996 |
| 0.5 | 0.1662 | 2.0 | 0.6309 | 3.5 | 0.9139 | 5.0 | 0.9917 | 6.5 | 0.9997 |
| 0.6 | 0.1994 | 2.1 | 0.6572 | 3.6 | 0.9241 | 5.1 | 0.9932 | 6.6 | 0.9998 |
| 0.7 | 0.2324 | 2.2 | 0.6825 | 3.7 | 0.9334 | 5.2 | 0.9944 | 6.7 | 0.9998 |
| 0.8 | 0.2653 | 2.3 | 0.7068 | 3.8 | 0.9418 | 5.3 | 0.9954 | 6.8 | 0.9999 |
| 0.9 | 0.2980 | 2.4 | 0.7302 | 3.9 | 0.9493 | 5.4 | 0.9963 | 6.9 | 0.9999 |
| 1.0 | 0.3305 | 2.5 | 0.7524 | 4.0 | 0.9561 | 5.5 | 0.9970 | 7.0 | 0.9999 |
| 1.1 | 0.3627 | 2.6 | 0.7736 | 4.1 | 0.9621 | 5.6 | 0.9975 | 7.1 | 0.9999 |
| 1.2 | 0.3946 | 2.7 | 0.7937 | 4.2 | 0.9674 | 5.7 | 0.9980 | 7.2 | 1.0000 |
| 1.3 | 0.4261 | 2.9 | 0.8126 | 4.3 | 0.9721 | 5.8 | 0.9984 | 7.3 | 1.0000 |
| 1.4 | 0.4572 | 2.9 | 0.8304 | 4.4 | 0.9762 | 5.9 | 0.9987 | 7.4 | 1.0000 |

## ***16.5.2 Blasius Skin Friction Coefficient***

The skin friction coefficient is defined by $cf = \dfrac{\mu \left.\dfrac{\partial u}{\partial y}\right|_{wall}}{\frac{1}{2}\rho_\infty u_\infty^2}$. For the Blasius Boundary layer $\dfrac{\partial u}{\partial y} = \dfrac{\partial^2 \psi}{\partial y^2} = u_\infty \sqrt{\dfrac{u_\infty}{\nu x}} f'' = u_\infty \sqrt{\dfrac{u_\infty}{\nu x}} \dfrac{\partial \phi}{\partial \eta}$. Thus, $cf = \dfrac{\mu \left.\dfrac{\partial u}{\partial y}\right|_{wall}}{\frac{1}{2}\rho_\infty u_\infty^2} = 2\nu \dfrac{u_\infty \sqrt{\dfrac{u_\infty}{\nu x}} \left.\dfrac{\partial \phi}{\partial \eta}\right|_{wall}}{u_\infty^2} = 2\sqrt{\dfrac{1}{\mathrm{Re}_x}} \left.\dfrac{\partial \phi}{\partial \eta}\right|_{wall}$,

with $\mathrm{Re}_x = \dfrac{u_\infty x}{\nu}$ From our numerical solution, listed in the above table, $\left.\dfrac{\partial \phi}{\partial \eta}\right|_{wall} = \left.\dfrac{\partial u'}{\partial \eta}\right|_{wall} = 0.333$ and we can then express the Blasius skin friction coefficient, as a function of $x$, by

$$cf = 0.666\sqrt{\frac{1}{\mathrm{Re}_x}} \tag{16.4}$$

### ***16.5.3 Laminar Boundary Layer Thickness***

From the above table the Blasius velocity reaches 99.9% of the freestream velocity at $\eta = 5$ for incompressible laminar flow. We can use this to estimate the thickness of the boundary layer as a function of $x$ if given the freestream density $\rho_\infty$, velocity $u_\infty$ and temperature $T_\infty$. The viscosity $\mu_\infty$ can be found using Sutherland/s formula in Section 15.2. The Reynolds number as a function of $x$ is $\mathrm{Re}_x = \dfrac{\rho_\infty u_\infty x}{\mu_\infty}$ and from the Blasius dimensionless coordinate

$$\eta = y\sqrt{\frac{u_\infty}{\nu_\infty x}} = \frac{y}{x}\sqrt{\frac{\rho_\infty u_\infty x}{\mu_\infty}} = \frac{y}{x}\sqrt{\mathrm{Re}_x}$$

we can estimate the boundary layer thickness by

$$y\big|_{\eta=5} \approx \delta(x) \approx \frac{5x}{\sqrt{\mathrm{Re}_x}}$$

Surprisingly, this estimate is fairly good even for supersonic freestreams.

## ***16.6 Exercise: Solve The TLNS Equations for Flow Past a Flat Plate***

Let $L$, the length of the plate, $M_\infty$ the free stream Mach number and $p_t$ and $T_t$, the total pressure and temperature, be given. The flow variables will be specified to approximate the conditions for near incompressible laminar flow so that we can compare the solution with the Blasius similarity solution obtained above. Let $M_\infty = 0.2$.The flat plate will be treated as an adiabatic wall.

### ***16.6.1 Exercise: Solve The TLNS Equations for Flow Past a Flat Plate***

***Initial conditions:***

The flow past a flat plate of length $L = 0.1m$ will start from rest. At t=0

$$u = 0,\ v = 0,\ p = p_t = 1\times10^5 N/m^2,\ T = T_t = 300^o K \text{ and } \rho = \rho_t = \frac{p_t}{RT_t} = \frac{p_t}{(\gamma-1)c_v T_t}$$

The pressure at the exit will be reduced to generate Mach 0.2 flow in the free stream. Using the isentropic flow relation (see Anderson, *Fundamentals of Aerodynamics*)

$$p_{exit} = p_t\left[1+\frac{\gamma-1}{2}M_\infty^2\right]^{\frac{-\gamma}{\gamma-1}} = 9.725\times10^4 N/m^2$$

***<u>The Mesh:</u>***

The mesh needs to be fine enough near the plate surface to support the viscous derivatives. Because the Reynolds number for aerodynamic flows is large, the mesh needs to very fine near the plate surface. We can estimate the Reynolds number as follows. As the program converges to steady state, the free stream pressure will adjust to $p_\infty = p_{exit}$ and the following isentropic relation can be used to determine $T_\infty$.

$$T_\infty = T_t\left[1+\frac{\gamma-1}{2}M_\infty^2\right]^{-1} = 297.62^o K$$

Using Sutherland's formula (Section 15.2), $\mu_\infty = 1.845\times10^{-5}\frac{N\cdot\sec}{m^2}$ and the equation of state $\rho_\infty = \frac{p_\infty}{(\gamma-1)c_v T_\infty} = 1.1462\,kg/m^3$, $c_\infty = \sqrt{\gamma p_\infty/\rho_\infty} = 344.64\,m/s$ and $u_\infty = c_\infty M_\infty = 68.93\,m/s$.

Therefore the Reynolds number, based on the plate length, is $\mathrm{Re}_L = \frac{\rho_\infty u_\infty L}{\mu_\infty} = 4.3\times10^5$ and the Reynolds number at a distance $x$ from the leading edge, at these flow conditions, is $\mathrm{Re}_x = \frac{\rho_\infty u_\infty x}{\mu_\infty} = 4.3\times10^6 x$. Using the formula in Section 16.5.3, the thickness of the boundary layer is estimated to be

$$\delta(x) = \frac{5x}{\sqrt{\mathrm{Re}_x}} = 2.4\times10^{-3}\sqrt{x}$$

The boundary layer thickness at $x = L/2$, the half plate length distance, is $\delta(L/2) = 5.4\times10^{-4}m$. The mesh should be fine over a distance $y_{fm} \ge \delta(L/2)$ from the plate surface to resolve the boundary layer in this region of the flow. Let the distance $y_{fm}$ be spanned by JLFM-1 mesh points in a finite volume mesh. The first mesh volume will lie within the plate itself to possibly implement boundary conditions and the surface itself is at $y_2 = 0$. We use the simple mesh stretching function of Section 5.3.1 to place the points, starting with spacing $y_3 - y_2 = \Delta y_{\min}$, across the boundary layer mesh.

$$y_j = y_{fm}\frac{e^{\kappa\frac{j-2}{JLFM-2}}-1}{e^{\kappa}-1}$$

The parameter $\kappa$ is determined by Newton's method for finding the value for which

$$f(\kappa) = \Delta y_{\min} - (y_3 - y_2) = \Delta y_{\min} - y_{fm}\frac{e^{\kappa\frac{1}{JLFM-2}}-1}{e^{\kappa}-1} = 0.$$

One column of the mesh at the leading edge of the flat plate is shown below, where $y_{fm} = 6.4\times10^{-4} m$, $JLFM = 22$ and $\Delta y_{\min} = 0.2 y_{fm}/(JLFM-2)$.

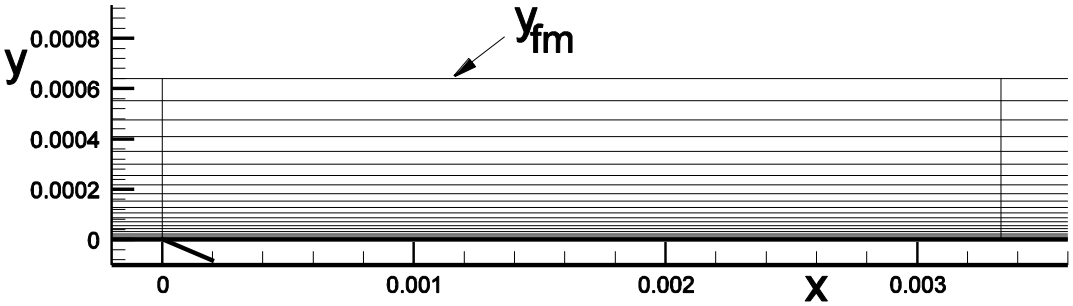


**Figure 16.13** Fine mesh detail near plate leading edge

The mesh covering only the boundary layer is very thin, as can be seen by the high cell aspect ratio $\Delta x/\Delta y$. Additional mesh points are needed above those shown in the figure to resolve the essentially inviscid region of flow outside the boundary layer region. This region is important to resolve because of the often significant inviscid-viscous interaction of the boundary layer with the external flow, such as flow separation. In our case, however, we wish to place the upper boundary of the flow far enough away from the boundary layer to avoid it having any effect on the boundary layer, such as a reflection at the top boundary of the compression waves created at the leading edge of the plate, caused by the flow suddenly adjusting to the "no slip" wall boundary condition. We would like to join a relatively coarse mesh to the fine boundary layer mesh seamlessly. We can use the formula given above to determine the mesh point spacing for $\Delta y_{\min}^{cm}$ for the coarse mesh, with the same value for $\kappa$.

$$\Delta y_{\min}^{cm} = y_{JLFM+1} - y_{JLFM} = y_{fm}\frac{e^{\kappa\frac{JLFM-1}{JLFM-2}}-1}{e^{\kappa}-1} - y_{fm}$$

Then, as before, we can stretch the mesh seamlessly to the top boundary, located at $y_{JL}$, using an additional $JL - JLFM$ mesh points.

$$y_j = (y_{JL} - y_{fm}) \frac{e^{\kappa_{cm} \frac{j-JLFM}{JL-JLFM}} - 1}{e^{\kappa_{cm}} - 1} + y_{fm},$$

where the parameter $\kappa_{cm}$ is determined by Newton's method for finding the value for which

$$f(\kappa_{cm}) = \Delta y_{\min}^{cm} - (y_{JLFM+1} - y_{JLFM}) = \Delta y_{\min}^{cm} - (y_{JL} - y_{fm}) \frac{e^{\kappa_{cm} \frac{1}{JL-JLFM}} - 1}{e^{\kappa_{cm}} - 1} = 0.$$

The joined mesh is shown below where $y_{JL} = L = 0.1m$ and $JL = 34$.

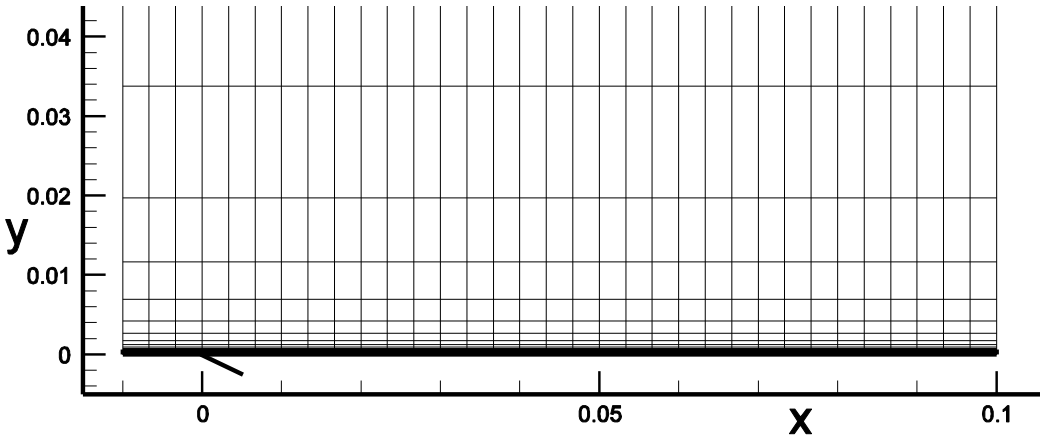


,

**Figure 16.14** Fine and coarse mesh near plate surface

The overall mesh is $I \times J = 34 \times 34$ for a finite volume mesh and $I \times J = 33 \times 33$ for a finite difference mesh, with 20 points spanning the fine mesh covering the boundary layer. There are 30 mesh points along the plate surface, $\Delta x = L/30$, and 4 upstream of the leading edge. The mesh is shown in Figures 16.13 and 16.14. The finite volume mesh was extended at the upstream and lower boundaries to include "ghost" volumes to be used for boundary conditions. For example, a set of grid points forming the "ghost" volumes were defined at the lower boundary by linear extrapolation, i.e., $x_{i,1} = 2x_{i,2} - x_{i,3}$ and $y_{i,1} = 2y_{i,2} - y_{i,3}$.

***Solution by Gauss-Seidel Line Relaxation***

The algorithm given in Section 16.3 yields a penta-diagonal matrix equation, which for each $i, j$ mesh point yields the following line of the matrix equation. (see also Chapter 11)

$$\overline{\mathrm{D}}_{i,j} \delta U_{i+1,j}^{n+1} + \overline{\mathrm{B}}_{i,j} \delta U_{i,j+1}^{n+1} + \overline{\mathrm{A}}_{i,j} \delta U_{i,j}^{n+1} + \overline{\mathrm{C}}_{i,j} \delta U_{i,j-1}^{n+1} + \overline{\mathrm{E}}_{i,j} \delta U_{i-1,j}^{n+1} = \Delta U_{i,j}^{n}$$

The block element matrices are defined for the Thin Layer Navier-Stokes equations in Section 16.3. There is no direct efficient inversion procedure for this matrix. Instead, we will use Gauss-Seidel relaxation to solve this equation, one column at a time, by sweeping through the mesh. Each

$i$ column of unknowns, $\left\{\delta U_{i,j}^{n+1}\right\}$, $j = 2,3,\cdots,JL-1$ will be solved for simultaneously as a tri-diagonal matrix equation with the off column unknowns evaluated using the latest available data, as described in Section 11.5.

$$\underbrace{\overline{\mathrm{B}}_{i,j}\delta U_{i,j+1}^{(k)} + \overline{\mathrm{A}}_{i,j}\delta U_{i,j}^{(k)} + \overline{\mathrm{C}}_{i,j}\delta U_{i,j-1}^{(k)}}_{block\ tridiagonal\ line\ terms} = \Delta U_{i,j}^{n} \underbrace{-\overline{\mathrm{D}}_{i,j}\delta U_{i+1,j}^{(*)} - \overline{\mathrm{E}}_{i,j}\delta U_{i-1,j}^{(**)}}_{Gauss-Seidel\ terms}$$

The tri-diagonal matrix equation, to be solved for each interior mesh point column $i$, is

$$\begin{bmatrix} \overline{\mathrm{A}}'_{i,J-1} & \overline{\mathrm{C}}_{i,J-1} & & & & & & \\ \overline{\mathrm{B}}_{i,J-2} & \overline{\mathrm{A}}_{i,J-2} & \overline{\mathrm{C}}_{i,J-2} & & & & & \\ & \ddots & \ddots & \ddots & & & & \\ & & \overline{\mathrm{B}}_{i,j} & \overline{\mathrm{A}}_{i,j} & \overline{\mathrm{C}}_{i,j} & & & \\ & & & \ddots & \ddots & \ddots & & \\ & & & & \overline{\mathrm{B}}_{i,3} & \overline{\mathrm{A}}_{i,3} & \overline{\mathrm{C}}_{i,3} & \\ & & & & & \overline{\mathrm{B}}_{i,2} & \overline{\mathrm{A}}'_{i,2} \end{bmatrix} \begin{bmatrix} \delta U_{i,J-1}^{n+1} \\ \vdots \\ \delta U_{i,j+1}^{n+1} \\ \delta U_{i,j}^{n+1} \\ \delta U_{i,j-1}^{n+1} \\ \vdots \\ \delta U_{i,2}^{n+1} \end{bmatrix} = \begin{bmatrix} \Delta U_{i,J-1}^{n} - \overline{\mathrm{D}}_{i,j}\delta U_{i+1,J-1}^{(*)} - \overline{\mathrm{E}}_{i,j}\delta U_{i-1,J-1}^{(**)} \\ \vdots \\ \Delta U_{i,j}^{n} - \overline{\mathrm{D}}_{i,j}\delta U_{i+1,j}^{(*)} - \overline{\mathrm{E}}_{i,j}\delta U_{i-1,j}^{(**)} \\ \vdots \\ \Delta U_{i,2}^{n} - \overline{\mathrm{D}}_{i,2}\delta U_{i+1,2}^{(*)} - \overline{\mathrm{E}}_{i,j}\delta U_{i-1,2}^{(**)} \end{bmatrix},$$

where the boundary conditions have been embedded into the top and bottom rows of the matrix.

***Boundary Conditions for the Viscous Terms:***

***At the plate surface -*** the no slip condition implies that the fluid velocity is zero downstream of the leading edge of the plate. The plate surface will be treated as an adiabatic wall. This assumes that the temperature at the plate surface has had enough time to come into equilibrium with fluid. The boundary conditions are similar to that given in Section 16.4.2 for Couette flow.

$$V_{i,1} = E_1 V_{i,2}, \quad \delta V_{i,1} = E_1 \delta V_{i,2}, \text{ and } E_1 = \begin{bmatrix} 1 & 0 & 0 & 0 \\ 0 & e & 0 & 0 \\ 0 & 0 & e & 0 \\ 0 & 0 & 0 & 1 \end{bmatrix}, \text{ where, } e = \begin{cases} 0, & finite\ difference \\ -1, & finite\ volume \end{cases}$$

***Ahead of the plate surface -*** Ahead of the leading edge, along the lower boundary of the mesh, the tangential velocity is symmetric across the boundary, as is the temperature.

$$E_1 = \begin{bmatrix} 1 & 0 & 0 & 0 \\ 0 & 1 & 0 & 0 \\ 0 & 0 & e & 0 \\ 0 & 0 & 0 & 1 \end{bmatrix}, \text{ where, } e = \begin{cases} 0, & finite\ difference \\ -1, & finite\ volume \end{cases}$$

***At the top boundary -*** The flow is treated as symmetric across the top boundary of the mesh, i.e., the centerline of a channel or a slip solid wall boundary. It is located far enough from the plate surface so that its effect on the boundary layer flow will be negligible

$$V_{i,J} = E_J V_{i,J-1},\ \ \delta V_{i,J} = E_J \delta V_{i,J-1}, \text{ and } E_J = \begin{bmatrix} 1 & 0 & 0 & 0 \\ 0 & 1 & 0 & 0 \\ 0 & 0 & e & 0 \\ 0 & 0 & 0 & 1 \end{bmatrix}, \text{ where, } e = \begin{cases} 0, \textit{ finite difference} \\ -1, \textit{ finite volume} \end{cases}$$

The implicit viscous boundary conditions shown above are imbedded inside of the matrix equation as was done for Couette flow in Section 16.4.2 by modifying main diagonal elements $\overline{\mathrm{A}}'_{i,2}$ and $\overline{\mathrm{A}}'_{i,J-1}$ and removing the viscous parts of elements $\overline{\mathrm{C}}_{i,2}$ and $\overline{\mathrm{B}}_{i,J-1}$. The next section for the Euler terms will further modify elements $\overline{\mathrm{A}}'_{i,2}$ and $\overline{\mathrm{A}}'_{i,J-1}$ and will also remove what is left in elements $\overline{\mathrm{C}}_{i,2}$ and $\overline{\mathrm{B}}_{i,J-1}$.

***<u>Boundary Conditions for the Euler Terms:</u>***

***At the lower and upper boundaries*** – Both these boundaries are, for the inviscid terms, streamline boundaries and the flow is symmetric with respect to them, mirror image symmetry. The velocity component normal to the wall vanishes, which implies "all you need is $p$" if the equations are written in conservation form. For the present problem these walls have no curvature and the boundary condition becomes simply $\dfrac{\partial p}{\partial y} = 0$. There is no need to use the Modified Steger-Warming or Roe algorithm to evaluate the Euler flux at the walls. Therefore,

***At the lower wall -*** $p_{i,1} = p_{i,2}$ and $G_{e_{i,\textit{lower boundary}}} = \begin{bmatrix} 0 \\ 0 \\ p_{i,2} \\ 0 \end{bmatrix}$

***At the upper wall -*** $p_{i,J} = p_{i,J-1}$ and $G_{e_{i,\textit{upper boundary}}} = \begin{bmatrix} 0 \\ 0 \\ p_{i,J-1} \\ 0 \end{bmatrix}$

This boundary condition is implemented in the implicit algorithm for the Thin Layer Navier-Stokes equations by replacing the Euler part of the flux term $G^n_{i,j-1/2}$ for $j = 2$ and $G^n_{i,j+1/2}$ for $j = J-1$ on the right hand side of Equation (16.1) as follows.

$$G^n_{Euler_{i,3/2}} \leftarrow G^n_{e_{i,\textit{lower boundary}}} \text{ and } \ G^n_{Euler_{i,J-1/2}} \leftarrow G^n_{e_{i,\textit{upper boundary}}}$$

Similarly, changes must also be made to the left hand side of Equation (16.1). In "delta law" form, the corresponding implicit approximation for either term is given by, where $k = 2$ or $k = J-1$,

$$\delta G_{e_{i,k}} = \begin{bmatrix} 0 \\ 0 \\ \delta p_{i,k} \\ 0 \end{bmatrix} = \left.\frac{\partial G_e}{\partial U}\right|_{i,k} \delta U_{i,k} = (\gamma - 1) \begin{bmatrix} 0 & 0 & 0 & 0 \\ 0 & 0 & 0 & 0 \\ \frac{u^2+v^2}{2} & -u & -v & 1 \\ 0 & 0 & 0 & 0 \end{bmatrix}_{i,k}^{n} \delta U_{i.k}$$

Embedding the boundary conditions in the above matrix equation requires that

$$\overline{\mathrm{A}}'_{i,2} = I + \frac{\Delta t}{\Delta x}\left(\alpha \overline{A}^{n}_{+_{i+1/2,2}} - \alpha \overline{A}^{n}_{-_{i-1/2,2}}\right) + \frac{\Delta t}{\Delta y}\left(\alpha \overline{B}^{n}_{+_{i,2+1/2}} - \alpha \left.\frac{\partial G}{\partial U}\right|_{i,2} + \frac{1}{\Delta y}\left(M_{yy_{i,2+1/2}} + M_{yy_{i,2-1/2}}(1-E_1)\right)N_{i,2}\right)$$

and

$$\overline{\mathrm{A}}'_{i,J-1} = I + \frac{\Delta t}{\Delta x}\left(\alpha \overline{A}^{n}_{+_{i+1/2,J-1}} - \alpha \overline{A}^{n}_{-_{i-1/2,J-1}}\right) + \frac{\Delta t}{\Delta y}\left(\alpha \left.\frac{\partial G}{\partial U}\right|_{i,J-1} - \alpha \overline{B}^{n}_{-_{i,J-3/2}} + \frac{1}{\Delta y}\left(M_{yy_{i,J-1/2}}(1-E_J) + M_{yy_{i,J-3/2}}\right)N_{i,J-1}\right)$$

***At the entrance and exit boundaries***- The flow is subsonic at both the entrance and exit. At the entrance $p_t$ and $T_t$ are given. Boundary conditions are given in Section 12.4.1 for this case. Assume that the flow enters parallel to the plate, i.e., $\theta = 0$. The semi-implicit boundary condition in Section 12.4.1.1 is the simplest to implement for determining $\delta U^{n+1}_{1,j}$ and $U^{n+1}_{1,j}$. Similarly, the procedure described in Section 12.5.1 can be used at the exit boundary. Note that these boundary conditions include only the Euler terms. This is consistent with our thin layer assumption, but is also used for the full Navier-Stokes equations for high Reynolds number flows. The subsonic flow boundary conditions are used at both the entrance and exit, even within the boundary layer at the exit. Later, we will simulate a boundary layer within a supersonic flow, where the flow near the wall is subsonic solely because of the viscous no-slip boundary condition. For this latter case the subsonic inviscid boundary condition of Section 12.5.1 is not appropriate and will require modification, as will be discussed in Section 16.10.

***2nd Order Accuracy for the Euler Terms: Rules of Reflection at Solid Boundaries***

The central differencing of the viscous terms described above is second order accurate. The Euler flux terms require values for $U$ at two points on either side of the surface at which the flux is to be calculated for second order accuracy (see the table in Section 9.11). At the mesh boundaries only one value of $U$ is known and the flux can be evaluated there as first order without jeopardizing the overall accuracy of the calculation (see Section 12.8). However, $U$ at the boundary point will be needed at the next flux surface near the boundary for second order accuracy. At inflow or outflow

boundaries $U$ is known, but a reflection rule is needed at no through flow boundaries, such as solid walls or stream line boundaries. Remember that $U$, the vector of conservative variables, is needed at the boundary for the Euler terms, which are inviscid, unlike $V$, which has been determined earlier at the boundaries for the viscous derivative terms. The viscous terms are already of second order accuracy. Now the Euler terms will be made so also. Consider either a solid wall or streamline boundary along the lower boundary. The reflection rule is the same for either boundary, namely mirror reflection of the flow across the boundary. Density, tangential momentum and energy are symmetric with respect to the boundary and normal momentum is asymmetric, i.e. $\frac{\partial \rho}{\partial n} = 0$, $\frac{\partial \rho u}{\partial n} = 0$, $\rho v = 0$ and $\frac{\partial e}{\partial n} = 0$ at the wall.

First, for the finite difference mesh we define $U$ at the mesh point $i,2$ located at the boundary.

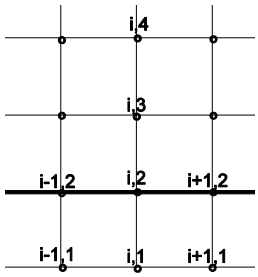

Finite difference mesh

$$U_{i,2} = \begin{bmatrix} \rho \\ \rho u \\ \rho v \\ e \end{bmatrix}_{i,2} = \underbrace{\begin{bmatrix} 1 & 0 & 0 & 0 \\ 0 & 1 & 0 & 0 \\ 0 & 0 & 0 & 0 \\ 0 & 0 & 0 & 1 \end{bmatrix}}_{E^0_{Euler}} \begin{bmatrix} \rho \\ \rho u \\ \rho v \\ e \end{bmatrix}_{i,3} = E^0_{Euler} U_{i,3}$$

Next applying the reflection rule for the mesh point $i,1$ located within the boundary.

$$U_{i,1} = \begin{bmatrix} \rho \\ \rho u \\ \rho v \\ e \end{bmatrix}_{i,1} = \underbrace{\begin{bmatrix} 1 & 0 & 0 & 0 \\ 0 & 1 & 0 & 0 \\ 0 & 0 & -1 & 0 \\ 0 & 0 & 0 & 1 \end{bmatrix}}_{E_{Euler}} \begin{bmatrix} \rho \\ \rho u \\ \rho v \\ e \end{bmatrix}_{i,3} = E_{Euler} U_{i,3}$$

The reflection rule for the finite volume approach, where mesh point $i,1$ is located at the center of the boundary "ghost" volume, is the same as above.

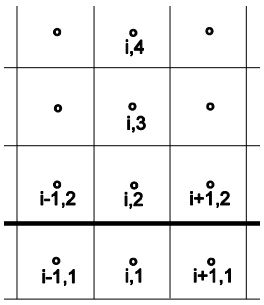

Finite volume mesh

$$U_{i,1} = \begin{bmatrix} \rho \\ \rho u \\ \rho v \\ e \end{bmatrix}_{i,1} = \underbrace{\begin{bmatrix} 1 & 0 & 0 & 0 \\ 0 & 1 & 0 & 0 \\ 0 & 0 & -1 & 0 \\ 0 & 0 & 0 & 1 \end{bmatrix}}_{E_{Euler}} \begin{bmatrix} \rho \\ \rho u \\ \rho v \\ e \end{bmatrix}_{i,2} = E_{Euler} U_{i,2}$$

Values for $U$ further across the boundaries can be determined, if required for higher order flux approximations. For example, $U_{i,0} = E_{Euler} U_{i,3}$ for both the finite difference and finite volume approaches.

***Time Step Size:***

Because all of the terms of the Thin Layer Navier-Stokes equations are to be treated implicitly there is no formal restriction on the size of the time step. However, the equations to be solved are non-linear and our matrix formulation contains a linearization at each time step. Therefore, caution should be exercised so that the Jacobian matrices do not change radically over one tine step. A reasonable choice is

$$\Delta t \approx cfl^n \left. \frac{\Delta x}{u + c} \right|_{1,J-1}^{n} \quad \text{with} \quad cfl^n = 2^{\frac{n-1}{4}}$$

Here, a 1-D explicit inviscid stability condition, using data at the upper boundary, is used to compute $\Delta t$ at each time step multiplied by a parameter, $cfl^n$, which starts at 1 and then doubles during each 4 time steps. The actual CFL number is the ratio of the time step used in the calculation to that given by Equation 16.3, which is many times larger than $cfl^n$. A maximum value or limit should be placed on the size of $cfl^n$ to avoid errors caused by adding and subtracting large numbers stored within finite sized computer" words". For example,

$$cfl^n = \min\left\{ 2^{\frac{n-1}{4}}, 10^4 \right\}$$

***Results:***

The velocity vector profiles, for every other $i^{th}$ column of mesh points, and the Mach 0.19 contour, $u/u_e = 0.95$, are shown in the figure below. Note that, unlike the Blasius solution, the no slip boundary condition is felt ahead of the leading edge through the subsonic flow.

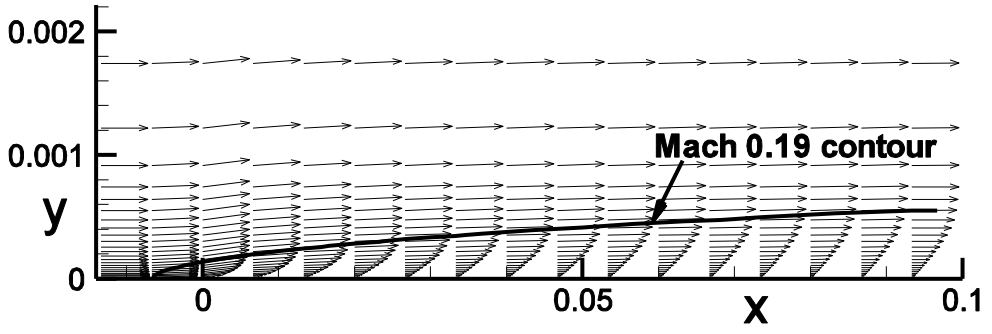


**Figure 16.15** Velocity vector profiles and Mach contour marking the boundary layer edge

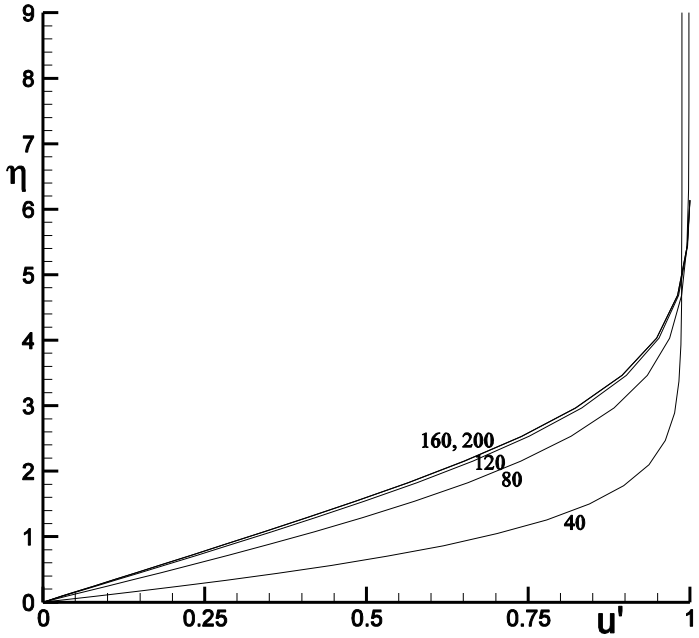


**Figure 16.16** Convergence of velocity profiles at $x_{20} = 0.05167m$, for time steps $n = 40, 80, 120, 160, 200$, $u' = u / u_\infty$

The velocity profiles near the plate center, using the Modified-Steger-Warming method, version 1, of 2nd order accuracy, are shown in Figure 16.16 converging to steady state. The 1st and 2nd order accurate Modified-Steger-Warming and the 2nd order accurate Roe method results are compared with the Blasius solution in Figure 16.17.

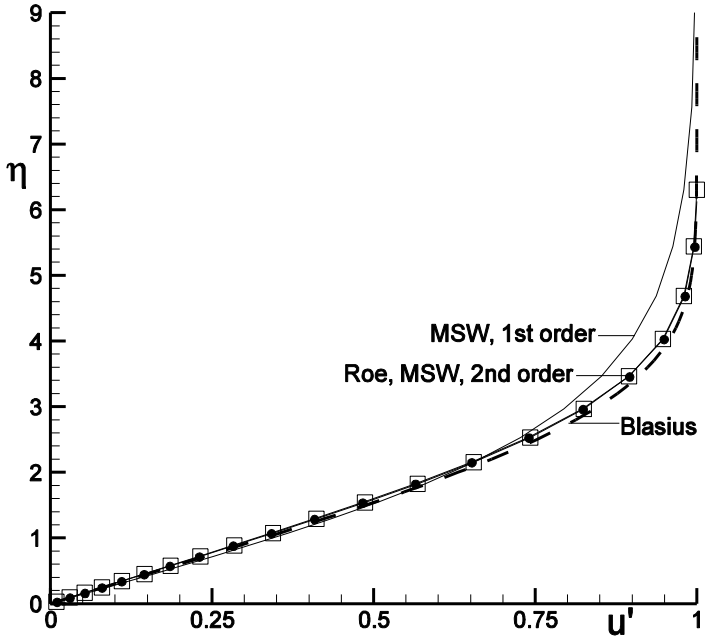


**Figure 16.17** Comparison of velocity profiles at $x_{20} = 0.05167m$

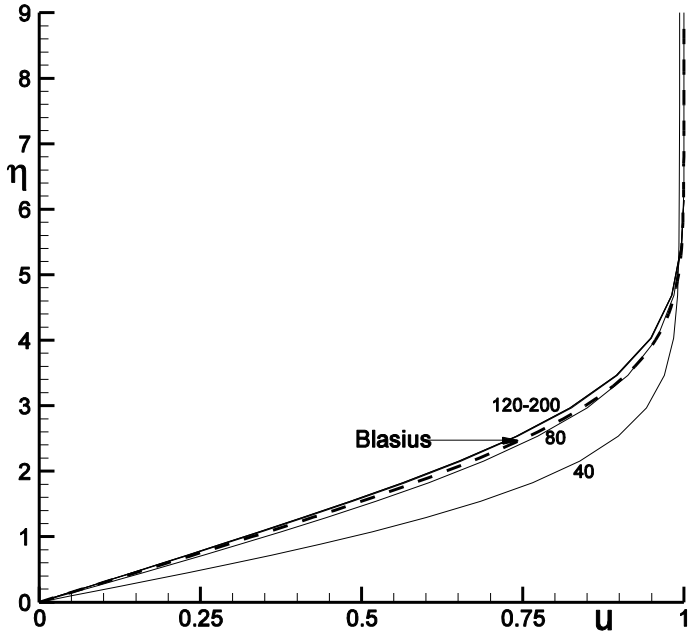


**Figure 16.18** Comparison of velocity profiles at $x_{20} = 0.05167m$ with uniform flow start

We could have started our solution with uniform Mach 0.2 flow, instead of at rest with a pressure gradient at the exit, in the hope of speeding up the calculation. Figure 16.18 shows that not much improvement is obtained starting with uniform flow.

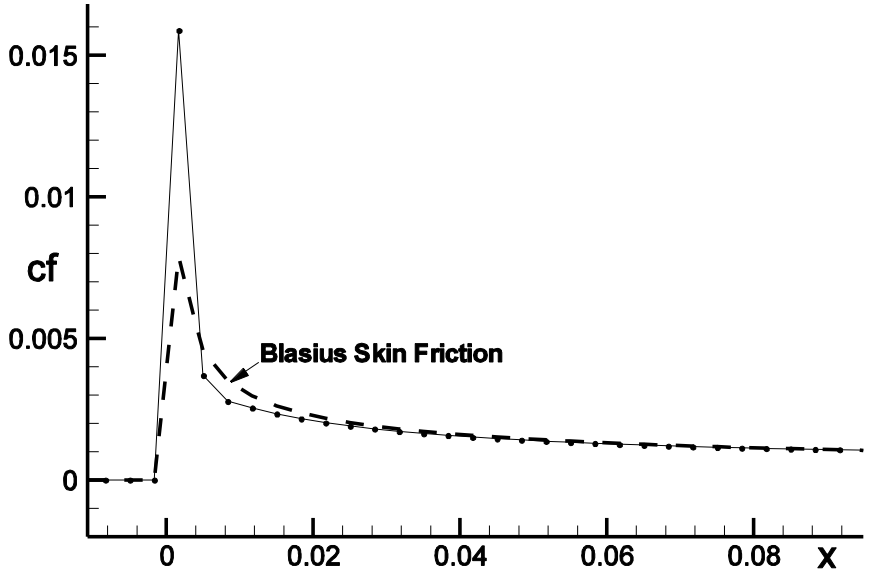


**Figure 16.19** Flat plate and Blasius skin friction comparison (400 time steps)

The skin friction results are compared in Figure 16.19 with the Blasius skin friction from Equation 16.4. Downstream of the leading edge the agreement is excellent. At the leading edge the mesh was not fine enough to resolve the boundary layer.

## ***16.7 The Full Navier-Stokes Equations***

The Navier-Stokes equations in two dimensions can be written as

$$\frac{\partial U}{\partial t}+\frac{\partial F}{\partial x}+\frac{\partial G}{\partial y}=0$$

where $U=\begin{pmatrix}\rho\\ \rho u\\ \rho v\\ e\end{pmatrix}$, $F=\begin{pmatrix}\rho u\\ \rho u^2+p-\tau_{xx}\\ \rho uv-\tau_{xy}\\ (e+p)u-\tau_{xx}u-\tau_{xy}v-k\dfrac{\partial T}{\partial x}\end{pmatrix}$, $G=\begin{pmatrix}\rho v\\ \rho vu-\tau_{yx}\\ \rho v^2+p-\tau_{yy}\\ (e+p)v-\tau_{yx}u-\tau_{yy}v-k\dfrac{\partial T}{\partial y}\end{pmatrix}$,

$$\tau_{xx}=2\mu\frac{\partial u}{\partial x}+\lambda(\frac{\partial u}{\partial x}+\frac{\partial v}{\partial y}),\quad \tau_{yy}=2\mu\frac{\partial v}{\partial y}+\lambda(\frac{\partial u}{\partial x}+\frac{\partial v}{\partial y})\quad\text{and}\quad \tau_{xy}=\tau_{yx}=\mu(\frac{\partial u}{\partial y}+\frac{\partial v}{\partial x})$$

We can express each flux term as the sum of an inviscid flux plus a viscous flux.

$$F=F_{Euler}+F_{viscous}\quad\text{and}\quad G=G_{Euler}+G_{viscous}$$

The viscous flux terms are

$$F_{viscous}=\begin{bmatrix}0\\ -\lambda\left(\dfrac{\partial u}{\partial x}+\dfrac{\partial v}{\partial y}\right)-2\mu\dfrac{\partial u}{\partial x}\\ -\mu\left(\dfrac{\partial u}{\partial y}+\dfrac{\partial v}{\partial x}\right)\\ -\tau_{xx}u-\tau_{xy}v-k\dfrac{\partial T}{\partial x}\end{bmatrix}\quad\text{or}\quad F_{viscous}=-M_{xx}\frac{\partial V}{\partial x}-M_{xy}\frac{\partial V}{\partial y}$$

with $V=\begin{bmatrix}\rho\\ u\\ v\\ T\end{bmatrix}$, $M_{xx}=\begin{bmatrix}0&0&0&0\\ 0&\lambda+2\mu&0&0\\ 0&0&\mu&0\\ 0&u(\lambda+2\mu)&v\mu&k\end{bmatrix}$ and $M_{xy}=\begin{bmatrix}0&0&0&0\\ 0&0&\lambda&0\\ 0&\mu&0&0\\ 0&v\mu&u\lambda&0\end{bmatrix}$

Similarly,

$$G_{viscous} = \begin{bmatrix} 0 \\ -\mu\left(\dfrac{\partial u}{\partial y}+\dfrac{\partial v}{\partial x}\right) \\ -\lambda\left(\dfrac{\partial u}{\partial x}+\dfrac{\partial v}{\partial y}\right)-2\mu\dfrac{\partial v}{\partial y} \\ -\tau_{xy}u-\tau_{yy}v-k\dfrac{\partial T}{\partial y} \end{bmatrix} \quad \text{or} \quad G_{viscous} = -M_{yx}\frac{\partial V}{\partial x} - M_{yy}\frac{\partial V}{\partial y}$$

$$\text{where} \quad M_{yx} = \begin{bmatrix} 0 & 0 & 0 & 0 \\ 0 & 0 & \mu & 0 \\ 0 & \lambda & 0 & 0 \\ 0 & v\lambda & u\mu & 0 \end{bmatrix} \quad \text{and} \quad M_{yy} = \begin{bmatrix} 0 & 0 & 0 & 0 \\ 0 & \mu & 0 & 0 \\ 0 & 0 & \lambda+2\mu & 0 \\ 0 & u\mu & v(\lambda+2\mu) & k \end{bmatrix}$$

## ***16.8 Implicit Algorithm for Navier-Stokes Equations***

An implicit algorithm for solving the Navier-Stokes equations is similar to that given earlier for the TLNS equations (see Equations16.1 and 16.2), except now all the viscous terms are to be included. The Euler terms are treated as before and all the viscous terms are centrally differenced about their respective flux surfaces. Note that only the pure $x$ and $y$ second derivatives are retained on the implicit side. This will be shown to be sufficient for maintaining numerical stability. The inclusion of the mixed derivatives on the implicit side would needlessly increase the size of the implicit mesh point stencil, and therefore the number of diagonals of the matrix equation to be inverted. The algorithm is

$$\begin{aligned} &\left\{ I + \alpha\Delta t\left( \frac{D_-\cdot}{\Delta x}\overline{A}^n_{+_{i+1/2,j}} + \frac{D_+\cdot}{\Delta x}\overline{A}^n_{-_{i-1/2,j}} + \frac{D_-\cdot}{\Delta y}\overline{B}^n_{+_{i,j+1/2}} + \frac{D_+\cdot}{\Delta y}\overline{B}^n_{-_{i,j-1/2}} \right) \right. \\ &\qquad \left. -\Delta t\left( \frac{D_-\cdot}{\Delta x}M_{xx_{i+1/2,j}}\frac{D_+\cdot}{\Delta x} + \frac{D_-\cdot}{\Delta y}M_{yy_{i,j+1/2}}\frac{D_+\cdot}{\Delta y} \right) N_{i,j} \right\} \delta U^{n+1}_{i,j} = \Delta U^{n+1}_{i,j} \\ &\qquad = -\Delta t\left( \frac{F^n_{i+1/2,j} - F^n_{i-1/2,j}}{\Delta x} + \frac{G^n_{i,j+1/2} - G^n_{i,j-1/2}}{\Delta y} \right)_{Euler} \\ &\qquad\quad + \Delta t\frac{D_-\cdot}{\Delta x}\left( M_{xx_{i+1/2,j}}\frac{D_+\cdot}{\Delta x}V_{i,j} + M_{xy_{i+1/2,j}}\frac{D_o\cdot}{\Delta y}\frac{1}{2}\left(V_{i,j}+V_{i+1,j}\right) \right) \\ &\qquad\quad + \Delta t\frac{D_-\cdot}{\Delta y}\left( M_{yx_{i,j+1/2}}\frac{D_o\cdot}{\Delta x}\frac{1}{2}\left(V_{i,j}+V_{i,j+1}\right) + M_{yy_{i,j+1/2}}\frac{D_+\cdot}{\Delta y}V_{i,j} \right) \end{aligned} \tag{16.5}$$

Similarly, the block element matrices are now defined as

$$\overline{\mathrm{A}}_{i,j} = I + \frac{\Delta t}{\Delta x_i}\left( \alpha \overline{A}^{n}_{+_{i+1/2,j}} - \alpha \overline{A}^{n}_{-_{i-1/2,j}} + \left( \frac{M_{xx_{i+1/2,j}}}{\Delta x_{i+1/2}} + \frac{M_{xx_{i-1/2,j}}}{\Delta x_{i-1/2}} \right) N_{i,j} \right)$$

$$+ \frac{\Delta t}{\Delta y_j}\left( \alpha \overline{B}^{n}_{+_{i,j+1/2}} - \alpha \overline{B}^{n}_{-_{i,j-1/2}} + \left( \frac{M_{yy_{i,j+1/2}}}{\Delta y_{j+1/2}} + \frac{M_{yy_{i,j-1/2}}}{\Delta y_{j-1/2}} \right) N_{i,j} \right), \qquad (16.6)$$

$$\overline{\mathrm{B}}_{i,j} = \frac{\Delta t}{\Delta y_j}\left( +\alpha \overline{B}^{n}_{-_{i,j+1/2}} - \frac{M_{yy_{i,j+1/2}}}{\Delta y_{j+1/2}} N_{i,j+1} \right), \qquad \overline{\mathrm{D}}_{i,j} = \frac{\Delta t}{\Delta x_i}\left( +\alpha \overline{A}^{n}_{-_{i+1/2,j}} - \frac{M_{xx_{i+1/2,j}}}{\Delta x_{i+1/2}} N_{i+1,j} \right),$$

$$\overline{\mathrm{C}}_{i,j} = \frac{\Delta t}{\Delta y_j}\left( -\alpha \overline{B}^{n}_{+_{i,j-1/2}} - \frac{M_{yy_{i,j-1/2}}}{\Delta y_{j-1/2}} N_{i,j-1} \right) \quad \textit{and} \quad \overline{\mathrm{E}}_{i,j} = \frac{\Delta t}{\Delta x_i}\left( -\alpha \overline{A}^{n}_{+_{i-1/2,j}} - \frac{M_{xx_{i-1/2,j}}}{\Delta x_{i-1/2}} N_{i-1,j} \right)$$

## ***16.9 Stability Analysis for the Implicit Navier-Stokes Algorithm***

The stability for the implicit algorithm applied to the Euler equations was discussed earlier in Section 9.11.1 for the case where first order accurate difference approximations were used on the implicit side of the equation, the left hand side, and second or third order accuracy was used on the explicit side of the equation, the right hand side. The algorithm was shown to be stable if the parameter $\alpha \geq \frac{3}{2}$. Actually, as shown later by Yung-Hung Wang, while a Stanford graduate student, the algorithm is stable for $\alpha \geq 1$. Values used for $\alpha$ usually fall in the range from 1 and 2.

The viscous terms have not yet been included in the analysis. Let's now confine our attention to these terms. It was stated earlier that the inclusion of only the pure *xx* and *yy* derivative approximation terms on the implicit side of the equation was sufficient for numerical stability to balance the complete set of pure and mixed derivative viscous terms on the explicit side of the equation. We will now discuss the proof of this statement. Consider the following equation obtained from Equation 16.5 by omitting all the spatial Euler terms and for convenience (and no loss in generality) using an equi-spaced Cartesian coordinate system.

$$\left\{ I - \Delta t\left( \frac{D_-\cdot}{\Delta x} M_{xx_{i+1/2,j}} \frac{D_+\cdot}{\Delta x} + \frac{D_-\cdot}{\Delta y} M_{yy_{i,j+1/2}} \frac{D_+\cdot}{\Delta y} \right) N_{i,j} \right\} \delta U^{n+1}_{i,j} = \Delta U^{n+1}_{i,j}$$

$$= \Delta t \frac{D_-\cdot}{\Delta x}\left( M_{xx_{i+1/2,j}} \frac{D_+\cdot}{\Delta x} V_{i,j} + M_{xy_{i+1/2,j}} \frac{D_o\cdot}{\Delta y} \frac{1}{2}\left( V_{i,j} + V_{i+1,j} \right) \right)$$

$$+ \Delta t \frac{D_-\cdot}{\Delta y}\left( M_{yx_{i,j+1/2}} \frac{D_o\cdot}{\Delta x} \frac{1}{2}\left( V_{i,j} + V_{i,j+1} \right) + M_{yy_{i,j+1/2}} \frac{D_+\cdot}{\Delta y} V_{i,j} \right)$$

Because of the top row of zero elements in each $M$ matrix, the continuity equation trivially becomes $\delta\rho^{n+1}_{i,j} = 0$. Also, the two momentum equations are only weakly coupled to the energy equation through the dependence of the viscosity coefficients $\lambda$ and $\mu$ on temperature $T$. Finally,

the energy equation has no cross derivative terms of $T$. Therefore, the stability of the above set of equations depends only upon the following reduced set.

$$\left\{I-\Delta t\left(\frac{D_-\cdot}{\Delta x}M'_{xx_{i+1/2,j}}\frac{D_+\cdot}{\Delta x}+\frac{D_-\cdot}{\Delta y}M'_{yy_{i,j+1/2}}\frac{D_+\cdot}{\Delta y}\right)\right\}\delta V'^{n+1}_{i,j}=$$

$$=\Delta t\frac{D_-\cdot}{\Delta x}\left(M'_{xx_{i+1/2,j}}\frac{D_+\cdot}{\Delta x}V'^{n}_{i,j}+M'_{xy_{i+1/2,j}}\frac{D_o\cdot}{\Delta y}\frac{1}{2}\left(V'^{n}_{i,j}+V'^{n}_{i+1,j}\right)\right)$$

$$+\Delta t\frac{D_-\cdot}{\Delta y}\left(M'_{yx_{i,j+1/2}}\frac{D_o\cdot}{\Delta x}\frac{1}{2}\left(V'^{n}_{i,j}+V'^{n}_{i,j+1}\right)+M'_{yy_{i,j+1/2}}\frac{D_+\cdot}{\Delta y}V'^{n}_{i,j}\right)$$

where

$$M'_{xx}=\frac{1}{\rho}\begin{bmatrix}\lambda+2\mu & 0\\ 0 & \mu\end{bmatrix},\ M'_{xy}=\frac{1}{\rho}\begin{bmatrix}0 & \lambda\\ \mu & 0\end{bmatrix},\ M'_{yx}=\frac{1}{\rho}\begin{bmatrix}0 & \mu\\ \lambda & 0\end{bmatrix},\ M'_{yy}=\frac{1}{\rho}\begin{bmatrix}\mu & 0\\ 0 & \lambda+2\mu\end{bmatrix}\text{ and }V'=\begin{bmatrix}u\\ v\end{bmatrix}$$

Transforming back from "delta law" form, this equation becomes

$$\left\{I-\Delta t\left(\frac{D_-\cdot}{\Delta x}M'_{xx_{i+1/2,j}}\frac{D_+\cdot}{\Delta x}+\frac{D_-\cdot}{\Delta y}M'_{yy_{i,j+1/2}}\frac{D_+\cdot}{\Delta y}\right)\right\}V'^{n+1}_{i,j}=$$

$$V'^{n}_{i,j}+\Delta t\left(\frac{D_-\cdot}{\Delta x}M'_{xy_{i+1/2,j}}\frac{D_o\cdot}{\Delta y}\frac{1}{2}\left(V'^{n}_{i,j}+V'^{n}_{i+1,j}\right)+\frac{D_-\cdot}{\Delta y}M'_{yx_{i,j+1/2}}\frac{D_o\cdot}{\Delta x}\frac{1}{2}\left(V'^{n}_{i,j}+V'^{n}_{i,j+1}\right)\right)$$

Using $V'_{i.j}=C_{l,m}e^{i\left(k_l x_i+k_m y_j\right)}$ as an arbitrary test component of the solution in the von Neumann stability analysis, where $C_{l,m}=\begin{bmatrix}c_1\\ c_2\end{bmatrix}_{l,m}$, we obtain the following equation for the numerical amplification factor $G_{l,m}$

$$\left\{I-\Delta tM'_{xx}\frac{2\left(\cos(k_l\Delta x)-1\right)}{\Delta x^2}-\Delta tM'_{yy}\frac{2\left(\cos(k_m\Delta y)-1\right)}{\Delta y^2}\right\}G_{l,m}=I-\Delta t\left(M'_{xy}+M'_{yx}\right)\frac{\sin(k_l\Delta x)}{\Delta x}\frac{\sin(k_m\Delta y)}{\Delta y}$$

.

or
$$G_{l,m}=\begin{bmatrix}\frac{1}{d_{11}} & \frac{-\frac{\Delta t}{\rho}(\lambda+\mu)\frac{\sin(k_l\Delta x)}{\Delta x}\frac{\sin(k_m\Delta y)}{\Delta y}}{d_{11}}\\ \frac{-\frac{\Delta t}{\rho}(\lambda+\mu)\frac{\sin(k_l\Delta x)}{\Delta x}\frac{\sin(k_m\Delta y)}{\Delta y}}{d_{22}} & \frac{1}{d_{22}}\end{bmatrix}$$

where $d_{11}=1+\frac{\Delta t}{\rho}\left((\lambda+\mu)\frac{2\left(1-\cos(k_l\Delta x)\right)}{\Delta x^2}+\mu\frac{2\left(1-\cos(k_m\Delta y)\right)}{\Delta y^2}\right)$

$$\text{and} \qquad d_{22} = 1 + \frac{\Delta t}{\rho}\left( (\lambda + \mu)\frac{2\left(1-\cos(k_m \Delta y)\right)}{\Delta y^2} + \mu \frac{2\left(1-\cos(k_l \Delta x)\right)}{\Delta x^2} \right)$$

The eigenvalues of $G_{l,m}$ are $\lambda_{\pm} = \frac{1}{2}\left(-b \pm \sqrt{b^2 - 4ac}\right)$, where

$$a = 1, \quad b = -\left(\frac{1}{d_{11}} + \frac{1}{d_{22}}\right) \quad \text{and} \quad c = \frac{1}{d_{11} d_{22}}\left\{1 - \left(\frac{\Delta t}{\rho}(\lambda + \mu)\frac{\sin(k_l \Delta x)}{\Delta x}\frac{\sin(k_m \Delta y)}{\Delta y}\right)^2\right\}.$$

Clearly $b < 0$ and $b^2 - 4ac$ can be shown to be equal to the sum of two positive terms.

$$b^2 - 4ac = \left(\frac{1}{d_{11}} - \frac{1}{d_{22}}\right)^2 + \frac{4}{d_{11} d_{22}}\left(\frac{\Delta t}{\rho}(\lambda + \mu)\frac{\sin(k_l \Delta x)}{\Delta x}\frac{\sin(k_m \Delta y)}{\Delta y}\right)^2$$

Therefore the eigenvalue of largest magnitude will occur for $\lambda_{+} = \frac{1}{2}\left(-b + \sqrt{b^2 - 4ac}\right)$. We can write $\lambda_{+} = 1 + \frac{1}{2}\left(-b - 2 + \sqrt{b^2 - 4ac}\right)$, where $-b - 2 < 0$. Then $\lambda_{+}$ will be less than one in magnitude if $(b+2)^2 > b^2 - 4ac$, which is fairly straight forward to show using the following trigonometric relation.

$$0 \le \sin^2\theta = 1 - \cos^2\theta = (1 + \cos\theta)(1 - \cos\theta) \le 2(1 - \cos\theta)$$

## ***16.10 The Interaction of a Shock Wave with a Boundary Layer***

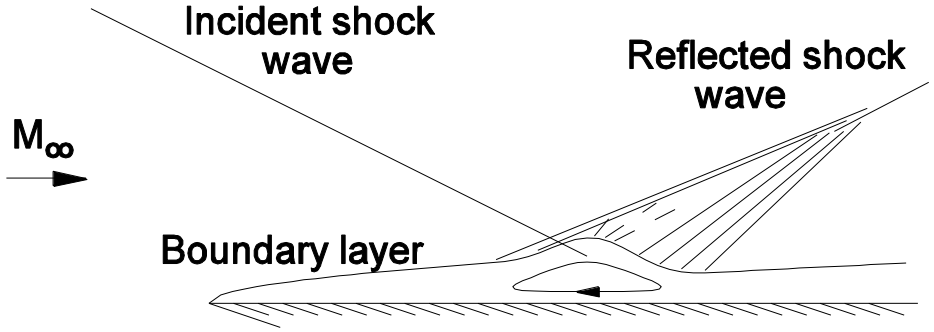


**Figure 16.20** Shock wave-boundary layer interaction

### ***16.10.1 Exercise: Solve The Navier-Stokes Equations for the Interaction of a Shock Wave with a Laminar Boundary Layer***

Given $L$, the distance from the leading edge of the flat plate to the position where an oblique shock wave of angle $\theta$ strikes the plate, $M_\infty$, the free stream Mach number, $T_t$, the total temperature and

$\mathrm{Re}_L$ the Reynolds number of the flow, calculate the interaction of the shock wave incident upon the boundary layer. The flat plate will be treated as an adiabatic wall.

***Initial conditions:***

$$L = 4.953\times10^{-2}\,m,\ M_\infty = 2.0,\ T_t = 300^o K,\ \mathrm{Re}_L = 2.96\times10^5 \text{ and } \theta = 32.585^o$$

These conditions correspond to an experiment by R.J. Hakkinen, L. Greger, L. Trilling and S.S. Arbarbanel at MIT in 1959. The oblique shock wave of angle $\theta = 32.585^o$ is chosen to increase the pressure after shock wave reflection from the plate surface by 40%,enough to cause boundary layer separation.

The free stream temperature is found from $T_\infty = T_t\left[1+\frac{\gamma-1}{2}M_\infty^2\right]^{-1} = 166.7^o K$. Using the equation of state and Sutherland's formula (Section 15.1), , $c_\infty = 257.9\,m/s$, $u_\infty = c_\infty M_\infty = 515.8\,m/s$ and $\mu_\infty = 1.132\times10^{-5}\,\frac{N\cdot\sec}{m^2}$. The Reynolds number can be used to find the free stream density, based on the plate length, is $\rho_\infty = \frac{\mathrm{Re}_L\,\mu_\infty}{u_\infty L} = 0.1312\,kg/m^3$. The free stream pressure is then $p_\infty = 6233\,N/m^2$. These conditions are used as the initial conditions for all interior mesh points.

The conditions behind an oblique shock wave of angle $\theta$ will be placed along the top boundary of the flow field, which will then feed air in during the calculation to form the incident shock wave. The solution for the conditions behind a normal shock wave is given in Section 13.2.2.1, and the equations for an oblique shock wave are given in Section 2.4.3.6. Note the correspondence between the velocity components normal to the oblique shock wave with those in Section 13.2.2.1.

From Section 2.4.3.6, the oblique shock relations for the steady Euler equations are, with $q_n = u\sin\theta - v\cos\theta$, $q_t = u\cos\theta + v\sin\theta$ and $p = (\gamma-1)\left(e - \frac{1}{2}\rho(q_n^2+q_t^2)\right)$,

$$\rho_2 q_{n2} = \rho_\infty q_{n\infty} = \rho_\infty u_\infty \sin\theta = m$$
$$\rho_2 q_{n2}^2 + p_2 = \rho_\infty q_{n\infty}^2 + p_\infty = n$$
$$\rho_2 q_{n2} q_{t2} = \rho_\infty q_{n\infty} q_{t\infty}$$
$$(e_2 + p_2)q_{n2} = (e_\infty + p_\infty)q_{n\infty} = mh$$

From Section 13.2.2.1the solution is

$$q_{t2} = q_{t\infty} = u_\infty\cos\theta = 434.6m \quad \text{and} \quad q_{n2} = \frac{-b+\sqrt{b^2-4ac}}{2a} = 245.8m\ ,$$

$$\text{where} \quad a = \frac{1}{2} - \frac{\gamma}{\gamma-1}, \quad b = \frac{\gamma}{\gamma-1}\frac{n}{m} \quad \text{and} \quad c = \frac{q_{t2}^2}{2} - h\,.$$

Therefore

$$\rho_2 = \frac{m}{q_{n2}} = 0.1482\, kg/m^3,$$
$$p_2 = n - mq_{n2} = 7397 N/m^2,$$
$$u_2 = \sin\theta q_{n2} + \cos\theta q_{t2} = 498.6\, m/s$$
$$v_2 = \cos\theta q_{n2} - \sin\theta q_{t2} = -26.93\, m/s$$

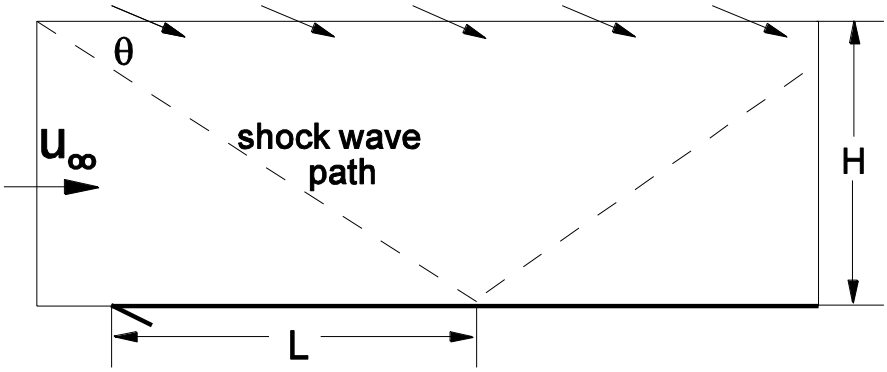


**Figure 16.21** Sketch of flow volume about shock wave-boundary layer interaction

***The Mesh:***

As before in Section 16.6 for viscous flow past a flat plate, the mesh needs to be fine enough near the plate surface to support the viscous derivatives that form the boundary layer and extend far enough above the plate to cover the incident shock wave. Again, we will use a stretched fine mesh covering the boundary layer and a coarse mesh, joined seamlessly, above.

We choose a finite difference grid containing 64 x 40 mesh points (or 65 x 41 finite volumes), equally spaced in the $x$ - direction, with 30 mesh spaces from the leading edge of the plate to $x = L$, $\Delta x = L/30$, and 6 mesh spaces ahead of the plate. We choose $H$, the height of the flow volume, such that the shock wave passes through the left top corner of the mesh.

$$H = (6\Delta x + L)\tan\theta = 3.8\times10^{-2} m$$

We use 20 stretched mesh points to span the fine mesh and 20 equi-spaced mesh points to cover the coarse mesh. There are two unknowns, the value of $\kappa$ used in the Rakich exponential stretching function and the location $y_{fm}$ at which the two meshes are to be joined seamlessly. We can estimate where it should be placed, as we did before in Section16.6

$$y_{fm} \approx \delta(L) = \frac{5L}{\sqrt{\mathrm{Re}_L}} = 4.55\times10^{-4} m$$

We choose for the minimum mesh spacing at the plate to be

$$\Delta y_{\min} = \delta(L)/30 = 1.52\times10^{-5} m$$

We now determine $\kappa$ and $y_{fm}$, under the above constraints, using a compound stretching, as follows.

## ***16.10.2 A Compound Stretching Function***

The first mesh point located at the plate surface is denoted by $y_2 = 0$, the spacing $\Delta y_{\min} = y_3 - y_2$ and $JLFM = 21$

$$y_j = y_{fm} \frac{e^{\kappa \frac{j-2}{JLFM-2}} - 1}{e^{\kappa} - 1}$$

We define the first equation, for which we need to find values for $\kappa$ and $y_{fm}$

$$f_1(\kappa, y_{fm}) = \Delta y_{\min} - (y_3 - y_2) = \Delta y_{\min} - y_{fm} \frac{e^{\kappa \frac{1}{JLFM-2}} - 1}{e^{\kappa} - 1} = 0.$$

The coarse mesh spacing is defined by, with $JL = 41$

$$\Delta y_{cm} = \frac{H - y_{fm}}{JL - JLFM}$$

We define a second function, such that $\Delta y_{cm}$ equals the spacing of the fine mesh if continued one more mesh point into the coarse mesh.

$$f_2(\kappa, y_{fm}) = \frac{H - y_{fm}}{JL - JLFM} - \left( y_{fm} \frac{e^{\kappa \frac{JLFM-1}{JLFM-2}} - 1}{e^{\kappa} - 1} - y_{fm} \right) = 0$$

We solve these two equations simultaneously using Newton's iteration method for vector functions.

$$A_k (X_{k+1} - X_k) = -F(X_k)$$

where the Jacobian matrix $A = \dfrac{\partial F}{\partial X}$ and the vectors $X = \begin{bmatrix} \kappa \\ y_{fm} \end{bmatrix}$ and $F = \begin{bmatrix} f_1(\kappa, y_{fm}) \\ f_2(\kappa, y_{fm}) \end{bmatrix}$

Notice the similarity to, or extension of, Newton's procedure for the scalar equation case. Starting with $X_1 = \begin{bmatrix} 1 \\ H/10 \end{bmatrix}$ and using 10 iterations is usually more than sufficient to find values for $\kappa$ and $y_{fm}$ that satisfy the two equations $f_1(\kappa, y_{fm}) = 0$ and $f_2(\kappa, y_{fm}) = 0$. For the present case $\kappa \to 4.666$ and $y_{fm} \to 5.7397 \times 10^{-3}$, which is larger than our estimate for $\delta(L)$ and is therefore acceptable.

The figure below shows a section of the fine mesh, near the plate leading edge, blending seamlessly into the outer course mesh.

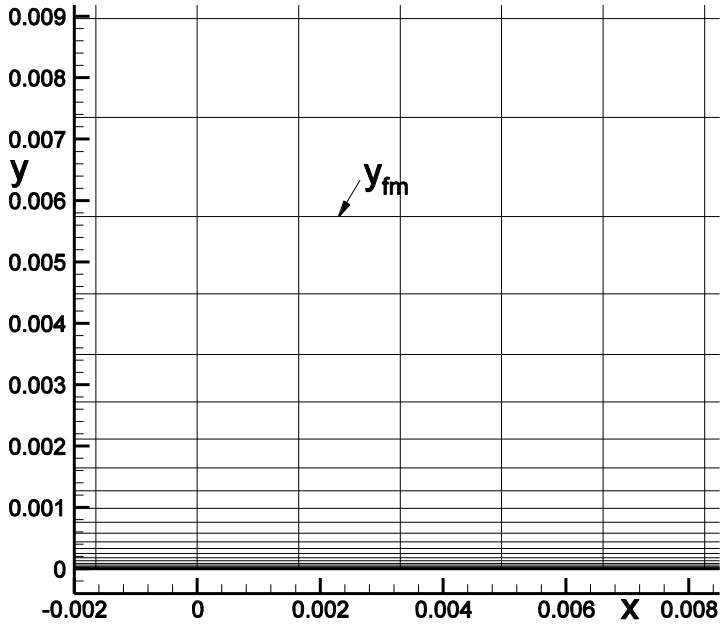


**Figure 16.22** Fine mesh near the leading edge of the flat plate

The figure below shows the complete mesh.

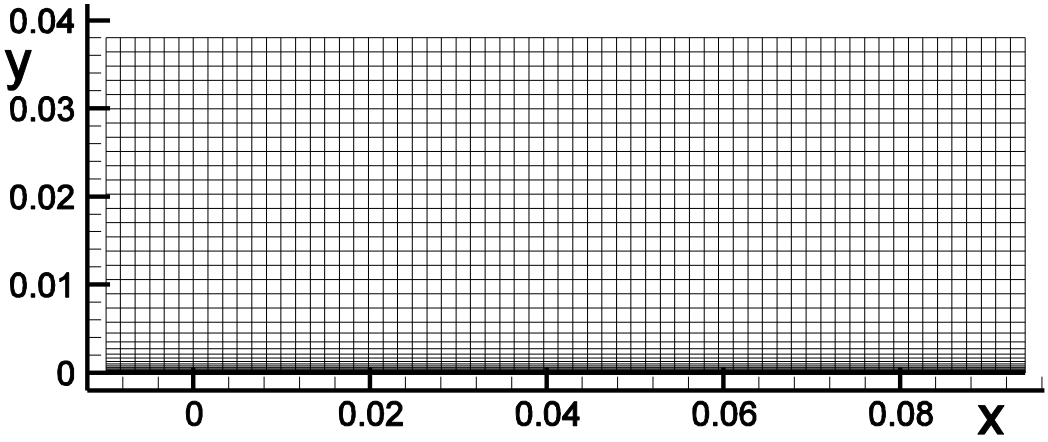


**Figure 16.23** Mesh for the shock wave – boundary layer interaction

***Boundary Conditions:***

The boundary condition procedures ahead of and along the plate surface are the same as those given in Section 16.6. The top boundary, where conditions for the incident shock are specified, is a flow through boundary and the fluxes along this boundary are treated similarly to a supersonic entrance boundary. The flow variables here are held fixed in time and, consequently, the elements of $\delta U_{i,JL}$ are set to zero. Note that the Jacobian matrices on the implicit side of matrix equation that

multiply $\delta U_{i,JL}$ need not be rigorously defined. The identity matrix would serve as well. The flow is supersonic at the entrance and far enough away from the leading edge of the flat plate so that $U_{1,j}$ may also be held fixed in time and, therefore $\delta U_{1,j} = 0$. The downstream boundary will also stay supersonic outside the boundary layer. Within the boundary layer, however, viscous stresses will smoothly join the outer inviscid flow to the stationary wall and the inner part of the boundary layer will be subsonic. A search can be made to find the value $j*$ within the boundary layer at the exit such that

$$M_{IL-1,j*-1} \le 1 \quad \text{and} \quad M_{IL-1,j*} > 1$$

For $j \ge j*$, the supersonic boundary conditions described in Section 12.5 can be used. For $j < j*$, the flow is subsonic because of viscous stress and the subsonic inviscid boundary condition procedures described in Section 12.5 are not suitable. However, the boundary layer region is said to be parabolic in the stream wise direction if it is attached and hence does not depend upon the flow downstream. A simple boundary condition at the exit within the subsonic portion of the boundary layer is to "shift" the solution from $IL-1$ to $IL$, i.e. $U_{IL-1,j} \to U_{IL,j}$ for $j < j*$. Errors made by this simple procedure will not be expected to travel upstream to adversely affect the solution, because of the parabolic nature of the boundary layer at the exit, even though subsonic flow exists along the wall. This same "shift" boundary condition procedure can actually be used for all values of $j$ at the exit for this exercise, because the supersonic nature of the flow at the exit also prevents errors from propagating upstream.

***Time Step Size:***

Because all of the terms of the Navier-Stokes equations are to be treated implicitly one would expect that there would be no formal restriction on the size of the time step. However, the solution contains a shock wave, a flow discontinuity, and it is impractical to choose a time step so large that the shock wave will try to move more that one mesh spacing per time step. Again, caution should be exercised so that the Jacobian matrices do not change radically over one tine step. A reasonable choice is

$$\Delta t \approx cfl^n \left.\frac{\Delta x}{u+c}\right|_{1,J-1}^{n} \quad \text{with} \quad cfl^n = 2^{\frac{n-1}{4}} cfl_0 \ ,$$

where $cfl_0 < 1$ is chosen to get the solution started. If too large a time step is chosen initially, the solution may quickly "blow up" because of the initial uniform flow trying to adjust immediately to the "no slip" wall boundary condition. The relatively large kinetic energy in the flow should be allowed some time to convert to internal energy by the action of the viscous stress at the wall. The wall pressure will then increase, moving fluid away from the wall, eventually reaching equilibrium with the external flow. Choosing too large of a time step would be like pouring gasoline on a hot plate. For the present exercise, a reasonable choice is

$$cfl_0 = 1/4 \text{ and } cfl^n = \min\left\{2^{\frac{n-1}{4}} cfl_0, 1\right\}$$

***Results:***

The following results were obtained using Gauss-Seidel Line Relaxation and the 2nd order Modified Steger-Warming method for 256 time steps. The 2nd order Roe results are similar, but 1st order for either method will not show separation on this mesh.

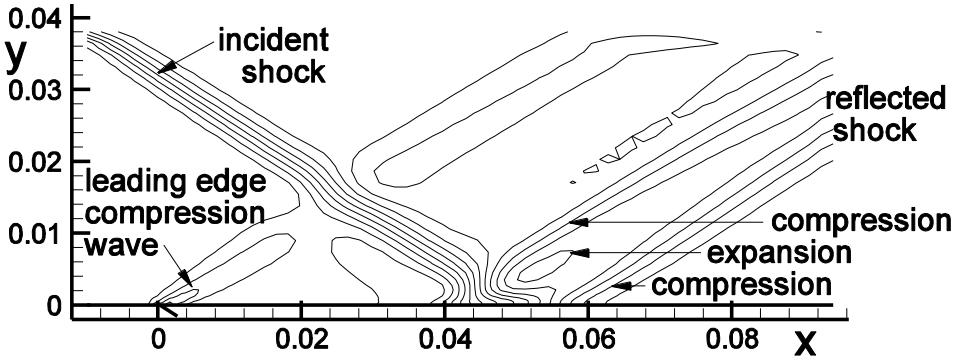


**Figure 16.24** Pressure contours for the shock wave – boundary layer interaction

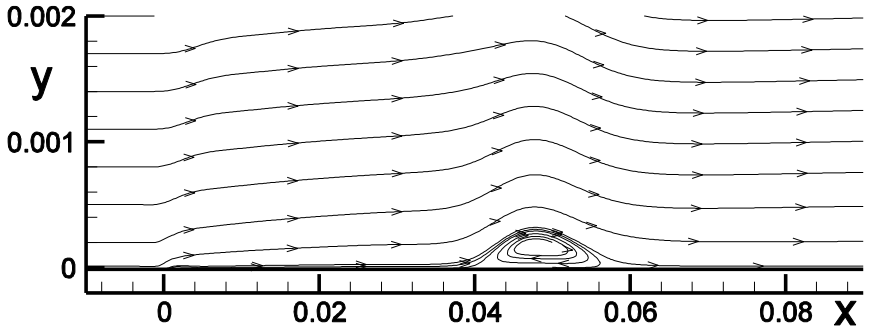


**Figure 16.25** Streamline traces within the boundary layer

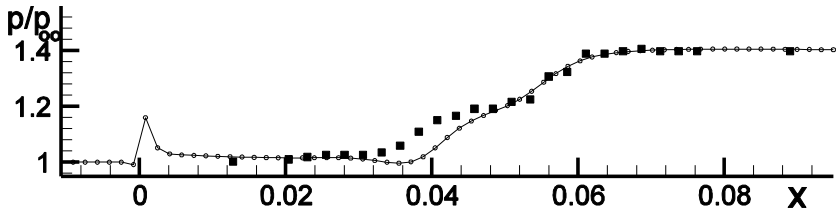


**Figure 16.26** Surface pressure, symbols indicate Hakkinen's data

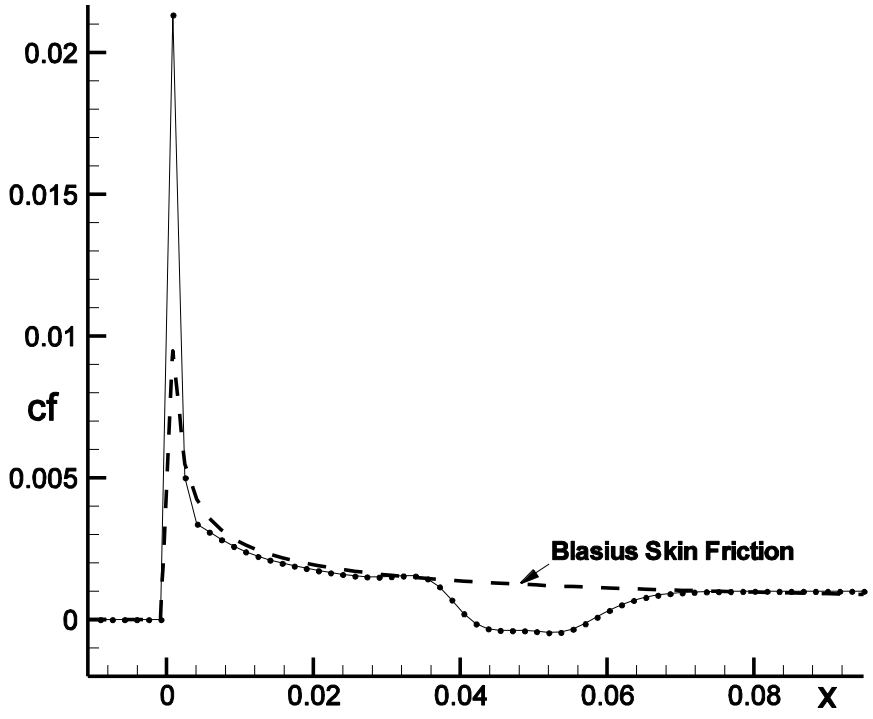


**Figure 16.27** Skin friction, $cf = \dfrac{\mu \left.\dfrac{\partial u}{\partial y}\right|_{wall}}{\frac{1}{2}\rho_\infty u_\infty^2}$, compared with Equation16.4

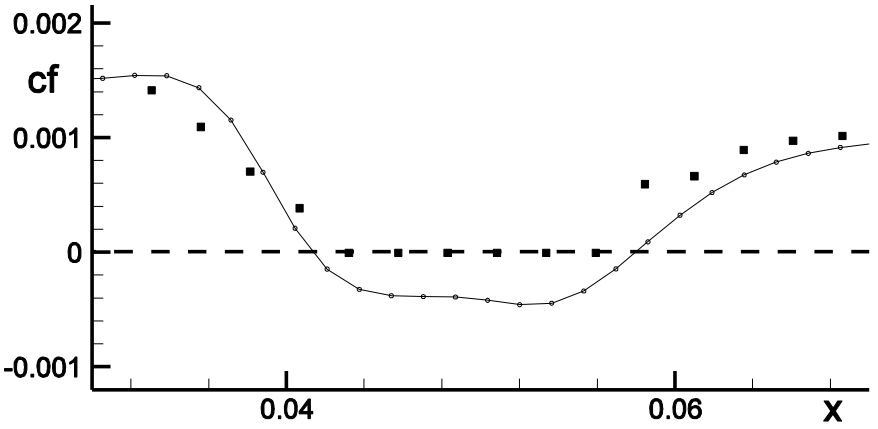


**Figure 16.28** Skin friction in the interaction region. Square symbols show Hakkinen data

Hakkinen's skin friction probe, located within a few thousandths of an inch above the plate, measured total pressure and hence velocity. It always faced upstream and could not measure the values for *cf* in the reversed flow region. These data points are plotted as zeros above. The length of the computed separation region agrees with the experimental data. Also shown in Figure 16.26 is the curve for the Blasius skin friction Equation 16.4, which agrees well with both the experiment and computation even though the flow is compressible. There is a compressibility correction for the Blasius formula, the Chapman-Rubesin constant, which would lower this curve by 4%.

Figures 16.29-31 show results for the 2nd order modified-Steger-Warming method on a 128x80 mesh covering the same flow volume. The incident shock wave, though still spread over three to five mesh intervals, appears sharper and the results for surface pressure and skin friction appear closer to Hakkinen's experimental results.

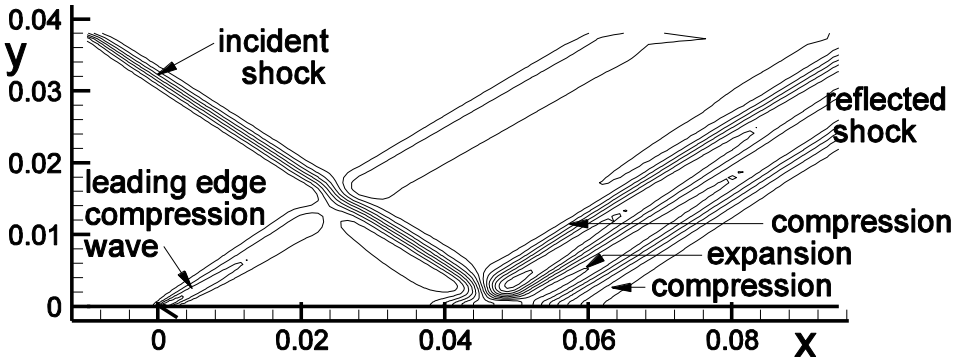


**Figure 16.29** Pressure contours for the shock wave – boundary layer interaction

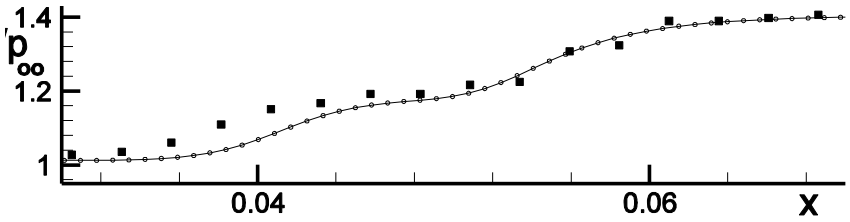


**Figure 16.30** Surface pressure in the interaction region. Square symbols show Hakkinen data

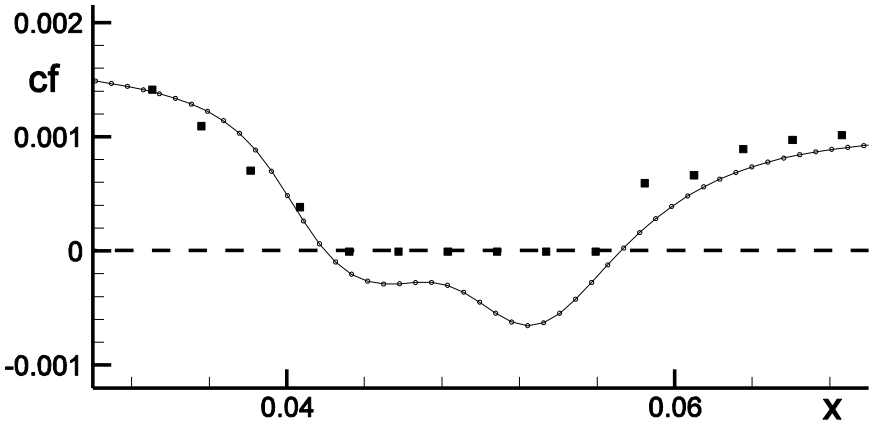


**Figure 16.31** Skin friction in the interaction region. Square symbols show Hakkinen data

## *16.11 Time Step Size, Time Accuracy and the CFL Number*

***Time Step Size and Time Accuracy:***

Above we have limited the time step to avoid allowing the shock to try to move more than one mesh spacing per time step. In Section 16.6 we allowed the time step to increase orders of magnitude larger. This was allowed because the low subsonic flow past the flat plate was very smooth. However, if the time step becomes very large the algorithm loses all pretense of time accuracy. The implicit method can be expressed as follows

$$\left\{ I + \Delta t \left( \frac{D \cdot \dfrac{\partial F}{\partial U}}{\Delta x} + \frac{D \cdot \dfrac{\partial G}{\partial U}}{\Delta y} \right) \right\} \delta U_{i,j} = -\Delta t \left( \frac{F^n_{i+1/2,j} - F^n_{i-1/2,j}}{\Delta x} + \frac{G^n_{i,j+1/2} - G^n_{i,j-1/2}}{\Delta y} \right) = -\Delta t \, \mathrm{F}(U^n_{i,j})$$

$$\text{or} \qquad \left\{ I + \Delta t \frac{\partial \mathrm{F}}{\partial U} \right\} \delta U_{i,j} = -\Delta t \, \mathrm{F}(U^n_{i,j})$$

As $\Delta t \to \infty$ the identity matrix within the brackets above, representing the time derivative, becomes insignificant and the equation reduces to

$$\frac{\partial \mathrm{F}}{\partial U} \delta U^{n+1}_{i,j} = -\mathrm{F}(U^n_{i,j}),$$

which again is Newton's method for determining the solution to $\mathrm{F}(U^n_{i,j}) = \left[\vec{0}\right]$, the steady state equation.

***<u>Time Step Size and the CFL Number:</u>***

From Equation 16.3 the maximum time step allowed by an explicit method is

$$\Delta t_{\text{explicit}} = \min_{i,j} \left\{ \frac{1}{\dfrac{|u_{i,j}|}{\Delta x} + \dfrac{|v_{i,j}|}{\Delta y} + c_{i,j} \sqrt{\dfrac{1}{\Delta x^2} + \dfrac{1}{\Delta y^2}} + 2\nu_{i,j} \left( \dfrac{1}{\Delta x^2} + \dfrac{2}{\Delta x \Delta y} + \dfrac{1}{\Delta y^2} \right)} \right\}$$

The true $CFL$ number of the calculation can be defined by

$$CFL = \frac{\Delta t_{\text{used}}}{\Delta t_{\text{explicit}}}$$

This number can be made artificially large by refining the mesh somewhere in the flow field, as for example near the wall in a viscous flow, rendering the number without real significance. A better unit of currency to judge the efficiency of the calculation is to measure how far the flow moves per time step relative to the mesh spacing, for example, $\dfrac{u_\infty \Delta t_{\text{used}}}{\Delta x}$, where $\Delta x$ is representative of the mesh spacing. A better estimate would be to use a characteristic length of the flow instead, for

example the body or plate length, $\frac{u_\infty \Delta t_{\text{used}}}{L}$. This last computational unit of merit can be used to estimate the number of steps, $N$, required to reach a steady state solution, assuming that $\Delta t_{\text{used}}$ is not chosen so large to lose all time accuracy in the calculation. A rule of thumb, for example, is that the flow time required for a supersonic flow to reach steady state is 3 to 5 times $t = L/u_\infty$, which would require $N = 3\,to\,5 \times \frac{L}{u_\infty \Delta t_{\text{used}}}$.